

# An assessment of ocean alkalinity enhancement using aqueous hydroxides: kinetics, efficiency, and precipitation thresholds

Mallory C. Ringham<sup>1</sup>, Nathan Hirtle<sup>1</sup>, Cody Shaw<sup>1</sup>, Xi Lu<sup>1</sup>, Julian Herndon<sup>2,3</sup>, Brendan R. Carter<sup>2,3</sup>, Matthew D. Eisaman<sup>4,5</sup>

<sup>1</sup>Stony Brook University, Stony Brook, NY, USA

<sup>2</sup>Cooperative Institute for Climate Ocean and Ecosystem Studies, University of Washington, Seattle, USA

<sup>3</sup>Pacific Marine Environmental Laboratory, National Oceanic and Atmospheric Administration, Seattle, WA, USA\*

<sup>4</sup>Department of Earth & Planetary Sciences, Yale University, New Haven, CT, USA

<sup>5</sup>Yale Center for Natural Carbon Capture, Yale University, New Haven, CT, USA

*Correspondence to:* Mallory Ringham (mallory.ringham@stonybrook.edu); Current address: Ebb Carbon Inc., San Carlos, CA, USA

## Abstract

Ocean alkalinity enhancement (OAE) is a promising approach to marine carbon dioxide removal (mCDR) that leverages the large surface area and carbon storage capacity of the oceans to sequester atmospheric CO<sub>2</sub> as dissolved bicarbonate (HCO<sub>3</sub><sup>-</sup>). One OAE method involves the conversion of salt in seawater into aqueous alkalinity (NaOH), which is returned to the ocean. The resulting increase in seawater pH and alkalinity causes a shift in dissolved inorganic carbon (DIC) speciation toward carbonate and a decrease in the surface-ocean pCO<sub>2</sub>. The shift in the pCO<sub>2</sub> results in enhanced uptake of atmospheric CO<sub>2</sub> uptake by the seawater due to gas exchange. In this study, we systematically test the efficiency of CO<sub>2</sub> uptake in seawater treated with NaOH at aquaria (15L) and tank (6000L) scales to establish operational boundaries for safety and efficiency in advance of scaling up to field experiments. CO<sub>2</sub> equilibration occurred on order of weeks to months, depending on circulation, air forcing, and air bubbling conditions within the test tanks. An increase of ~0.7-0.9 mol DIC/ mol added alkalinity (in the form of NaOH) was observed through analysis of seawater bottle samples and pH sensor data, consistent with the value expected given the values of the carbonate system equilibrium calculations for the range of salinities and temperatures tested. Mineral precipitation occurred when the bulk seawater pH exceeded 10.0 and  $\Omega_{\text{aragonite}}$  exceeded 30.0. This precipitation was dominated by Mg(OH)<sub>2</sub> over hours to 1 day before shifting to CaCO<sub>3, aragonite</sub> precipitation. These data, combined with models of the dilution and advection of alkaline plumes, will allow for estimation of the amount of carbon dioxide removal expected from OAE pilot studies. Future experiments should better approximate field conditions including sediment interactions, biological activity, ocean circulation, air-sea gas exchange rates, and mixing-zone dynamics.

## Keywords

Ocean Alkalinity Enhancement (OAE); marine carbon dioxide removal (mCDR); ocean carbon dioxide removal (ocean CDR)

## 1 Introduction

The Sixth Assessment Report of the Intergovernmental Panel on Climate Change reported that in addition to a drastic decrease in CO<sub>2</sub> emissions, active removal of 5-15 Gt of atmospheric CO<sub>2</sub> per year by 2100 is necessary to constrain average global warming to less than 1.5 - 2 °C (noting that the magnitude of carbon removals varies by

42 climate scenario: IPCC, 2022; Rogelj, 2018). A wide variety of negative emissions technologies (NETs) are under  
43 development to meet this enormous challenge (Minx et al., 2018; NASEM, 2019; NASEM, 2021; Rueda et al.,  
44 2021; Vitillo et al., 2022).

45 A suite of promising approaches to CO<sub>2</sub> removal termed ocean or marine carbon dioxide removal (ocean CDR or  
46 mCDR, respectively) leverage the enormous surface area and carbon storage capacity of the ocean (Boettcher et al.,  
47 2019; NASEM, 2021). Ocean alkalinity enhancement (OAE) is an mCDR method that aims to store atmospheric  
48 CO<sub>2</sub> in a dissolved phase in the ocean as bicarbonate ions (HCO<sub>3</sub><sup>-</sup>), thereby accelerating a natural planetary CO<sub>2</sub>  
49 regulation mechanism, the carbonate-silicate cycle (Berner, 1983; Isson et al., 2020). OAE has the potential to scale  
50 to gigatons of CO<sub>2</sub> removal per year (He and Tyka, 2023), but development of this approach requires careful  
51 consideration of: the methods and materials used to source and process alkalinity; the form and method of delivery  
52 of alkalinity to the surface ocean (for example, aqueous or solid phase); and selection of appropriate geographic sites  
53 for alkalinity dispersal (Oschlies et al., 2023). OAE methods under exploration include: mining and crushing  
54 alkaline minerals (e.g., olivine, basalts) to be spread via ship or in coastal environments (e.g., beach restoration, or  
55 salt marsh distribution) (Feng et al., 2017; Köhler, Hartmann, and Wolf-Gladrow, 2010; Monserrat et al., 2018;  
56 Rigopoulos et al., 2018); the mining or industrial production of Mg(OH)<sub>2</sub> or mining CaCO<sub>3</sub> and calcining it to CaO  
57 or Ca(OH)<sub>2</sub>, with the Mg(OH)<sub>2</sub> or Ca(OH)<sub>2</sub> spread via ship or coastal outfall pipe (Harvey, 2008; Ilyina et al., 2013;  
58 Kheshgi, 1995; La Plante, 2023; Moras et al., 2022; Nduagu, 2012; Rau, 2008; Renforth and Henderson, 2017;  
59 Shaw, 2022); and the electrochemical conversion of saltwater into aqueous hydroxides and dispersal via coastal  
60 outfalls (de Lannoy et al., 2018; Eisaman et al., 2018; Lu et al., 2022; Tyka, Van Arsdale, and Platt, 2022; Eisaman  
61 et al., 2023).

62 Many of these approaches and technologies are at a nascent stage. We must move quickly to quantitatively test and  
63 characterize their performance to determine which, if any, justify larger-scale deployment. The electrochemical  
64 conversion of salt (NaCl) into aqueous alkalinity (NaOH) has many potential advantages in scaling considerations,  
65 including simplified distribution of a liquid product to the ocean, avoidance of mining and the transportation of the  
66 alkalinity source over long distances, and avoidance of potentially harmful impurities present in mined alkalinity  
67 sources (NASEM, 2021; Caserini, Storni, and Grosso, 2022).

68 Total alkalinity (TA) is defined as the excess of proton acceptors over proton donors in an aqueous solution (Eq. 1),  
69 where ellipses represent neglected acids and bases (Dickson 1981; Dickson 1992; Wolf-Gladrow et al., 2007). A  
70 higher TA value for a seawater sample indicates that it has a higher buffering capacity than a sample with a lower  
71 TA value. That is, for sample with a higher TA value, the addition of a given amount of acid to the sample will  
72 decrease its pH less than for a sample with a lower TA value.

$$73 \quad \text{TA} = [\text{HCO}_3^-] + 2 [\text{CO}_3^{2-}] + [\text{B}(\text{OH})_4^-] + [\text{OH}^-] + [\text{HPO}_4^{2-}] + 2 [\text{PO}_4^{3-}] + \dots - [\text{H}^+] - [\text{HSO}_4^-] - \dots \quad (1)$$

74 From Eq. (1), we see the increased OH<sup>-</sup> concentration in a treated seawater solution corresponds to a salt solution  
75 with increased alkalinity relative to the starting salt solution. This increase in OH<sup>-</sup> ion concentration rapidly  
76 increases the seawater pH upon mixing, resulting in a shift of the dissolved inorganic carbon (DIC) speciation  
77 towards carbonate (Eisaman et al., 2023):



80 The concentration of dissolved CO<sub>2</sub> gas (CO<sub>2, aq</sub>) in this alkalinity-enhanced seawater is less than it would be if it  
81 were in equilibrium with atmospheric CO<sub>2</sub> (Equation 2b). Over the longer timescale required for air-sea gas  
82 exchange - weeks to months (Wang et al., 2023) or months to years (He and Tyka, 2023) depending on location - the  
83 disequilibrium in the surface ocean resulting from the alkalinity addition drives the invasion of atmospheric CO<sub>2</sub>  
84 into seawater (or lessens the outgassing of CO<sub>2</sub> from the surface ocean to the atmosphere), where it reacts with

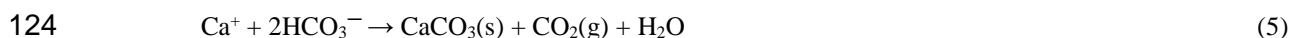
85 carbonate and is stored primarily in the stable bicarbonate phase (Jones et al., 2014; Bach et al., 2023; Renforth and  
86 Henderson, 2017; Eisaman et al., 2023).



89 Under typical ocean conditions, after equilibrium has been reached, OAE results in an increase in the DIC in  
90 seawater on the order of 0.7-0.9 moles of DIC per mole of NaOH added, with a slightly increased pH relative to the  
91 initial value (He and Tyka, 2023).

92 It is possible that air-sea gas exchange will not completely drive the seawater  $p\text{CO}_2$  to the initial unperturbed value  
93 before the seawater sinks into the ocean interior and loses contact with the atmosphere for hundreds to thousands of  
94 years. Therefore, the DIC anomaly relative to the alkalinity anomaly present when the seawater sinks into the ocean  
95 interior may be used to assess the effective impact of the OAE for capturing atmospheric  $\text{CO}_2$  on the 0-100 year  
96 timescales that are most important for climate interventions.

97 In addition to the storage of atmospheric  $\text{CO}_2$  in the form of DIC, this process may have the potential to locally and  
98 transiently mitigate the elevated  $p\text{CO}_2$  associated with ocean acidification (NASEM, 2021; Cross et al., 2023;  
99 Butenschön et al., 2021). In a water body with a finite seawater exchange rate with the ocean, such as a semi-  
100 protected estuary or bay, alkalinity could be added in a controlled manner such that the combination of the rapid  
101 reactions described by Eq.(1) and the exchange/flushing rate with the open ocean result in the bay being held in  
102 steady-state at a target pH or aragonite saturation state value that is higher than its equilibrium value under  
103 conditions of ocean acidification. As this added alkalinity diffuses through the bay and makes its way to the open  
104 ocean,  $\text{CO}_2$  removal and storage as DIC would occur. By metering the rate of alkalinity addition to the bay to match  
105 the flushing rate, the pH or saturation state of the bay can be held at a constant target value. Even once equilibrium  
106 has been achieved in the open ocean, the pH and the carbonate ion concentration in the open ocean remains slightly  
107 higher than before the alkaline discharge. However, the absolute value of this pH increase after equilibrium has been  
108 reached is sufficiently small relative to the alkalinity and DIC increase that mitigating ocean acidification on a  
109 global scale with this method is unfeasible. For example, increasing the equilibrium pH value from 8.0 to 8.1 at a  
110 fixed  $p\text{CO}_2$  of 400  $\mu\text{atm}$  (at 20 C and 35 salinity with no macronutrients) requires a TA increase of around  $\sim 620$   
111  $\mu\text{mol/kg-sw}$  and a DIC increase of around 520  $\mu\text{mol/kg-sw}$ . Using these numbers, mitigating OA over the entire 360  
112 million  $\text{km}^2$  surface of the ocean to a depth of 100 meters would require around 487 gigatons of cumulative  $\text{CO}_2$   
113 removal. Deploying SEA MATE in the ocean or coastal waters will require an understanding of carbonate chemistry  
114 in seawater in the ocean volume under consideration, as well as thresholds for safe operation. For example, at the  
115 point of alkaline dispersal where there is the maximum change in seawater chemistry, SEA MATE must control the  
116 rate of alkalinity addition relative to the rate of mixing and dilution in the ocean to avoid the precipitation of  
117  $\text{Mg}(\text{OH})_2$  or  $\text{CaCO}_3$  (Hartmann et al., 2023; Moras et al., 2022). While  $\text{Mg}(\text{OH})_2$  readily redissolves, an increase in  
118 turbidity due to precipitation may negatively affect marine organisms (Bainbridge et al., 2018; Broderson et al.,  
119 2017). By contrast,  $\text{CaCO}_3$  will generally not redissolve in the surface ocean without biological mediation, and  
120 runaway precipitation, where alkalinity removed by precipitation exceeds that added by the OAE treatment, can  
121 occur under conditions of increased aragonite saturation state and increased nucleation sites in the water column  
122 (Moras et al., 2022).  $\text{CaCO}_3$  precipitation could counteract the intended effect of the OAE intervention by removing  
123 alkalinity from the surface ocean and releasing  $\text{CO}_2$  gas via Eq. 5 (Zeebe and Wolf-Gladrow, 2001):



125 Upon dispersal to the ocean through a coastal outfall pipe, the added alkalinity is advected and diffuses away from  
126 the point source, becoming increasingly diluted through the mixing zone. Because the timescale for air-sea gas  
127 exchange and re-equilibration described by Eq. (2) is longer than the characteristic timescale for dilution driven by

128 tides, currents, and weather, most of the CO<sub>2</sub> removal occurs far from the mixing zone. Dilution will spread the  
129 impacts over a broad area, to an extent that it is unlikely that the impacts on the DIC distribution can be quantified  
130 using only direct measurements, given current instrument resolution and the typical dynamic range of natural  
131 variability (Wang et al., 2023). In general, options for measurement, reporting, and verification (MRV) of OAE will  
132 therefore rely on (Ho et al., 2023): experimentation in laboratory and mesocosm settings, such as the work we  
133 describe here, to establish CO<sub>2</sub> removal dynamics under conditions of OAE; direct monitoring of the rate and  
134 characteristics of alkalinity addition into seawater; monitoring the seawater carbonate and environmental chemistry  
135 in the immediate vicinity of the outfall via sensors and sampling (Cyronak et al., 2023; Schulz et al., 2023); and  
136 ocean modeling to estimate CDR beyond the range of direct detection (Fennel et al., 2023).

137 While some work has investigated various aspects of NaOH-based ocean alkalinity enhancement in microcosms  
138 (Ferderer et al., 2022; Hartmann et al., 2023), and mesocosms (Groen et al., 2023), and other work has studied the  
139 release of NaOH over natural coral reefs as a method of local ocean acidification mitigation (Albright et al., 2016), a  
140 systematic characterization of the efficiency and kinetics of OAE as a function of key process parameters has not yet  
141 been performed. Here we report the first tank-scale tests of OAE that use aqueous hydroxide (NaOH) to enhance the  
142 alkalinity of natural seawater, a process that mimics OAE via the electrochemical brine-to-alkalinity conversion  
143 used in the SEA MATE process. Our experiments, conducted in 6,000 liter tanks using seawater pumped from Flax  
144 Pond on Long Island Sound in Stony Brook NY, quantify the magnitude and timescale of the CO<sub>2</sub> removal from the  
145 air and storage as seawater DIC by monitoring the air-seawater re-equilibration after an initial alkalinity  
146 perturbation. In addition, our use of both laboratory-processed bottle samples and field-deployable sensors to  
147 measure and over-constrain the carbonate chemistry response allows us to assess the suitability of certain sensing  
148 platforms for MRV. Finally, we investigate safe thresholds for the rate and concentration of alkalinity addition to  
149 avoid: (1) the precipitation and redissolution of Mg(OH)<sub>2</sub> that can lead to local, temporary increases in turbidity; and  
150 (2) the precipitation of CaCO<sub>3</sub>, which partially reverses the intended OAE effect by removing alkalinity from, and  
151 releasing CO<sub>2</sub> gas into, the surrounding seawater.

152 Using this approach, we address the following key questions:

153 (1) How much additional atmospheric CO<sub>2</sub> is stored in seawater as DIC in response to a given alkalinity  
154 perturbation?

155 (2) What is the timescale for CO<sub>2</sub> removal from the air, and how does it depend on pH and the magnitude of  
156 alkalinity enhancement?

157 (3) What are the conditions for Mg(OH)<sub>2</sub> precipitation upon addition of NaOH to seawater?

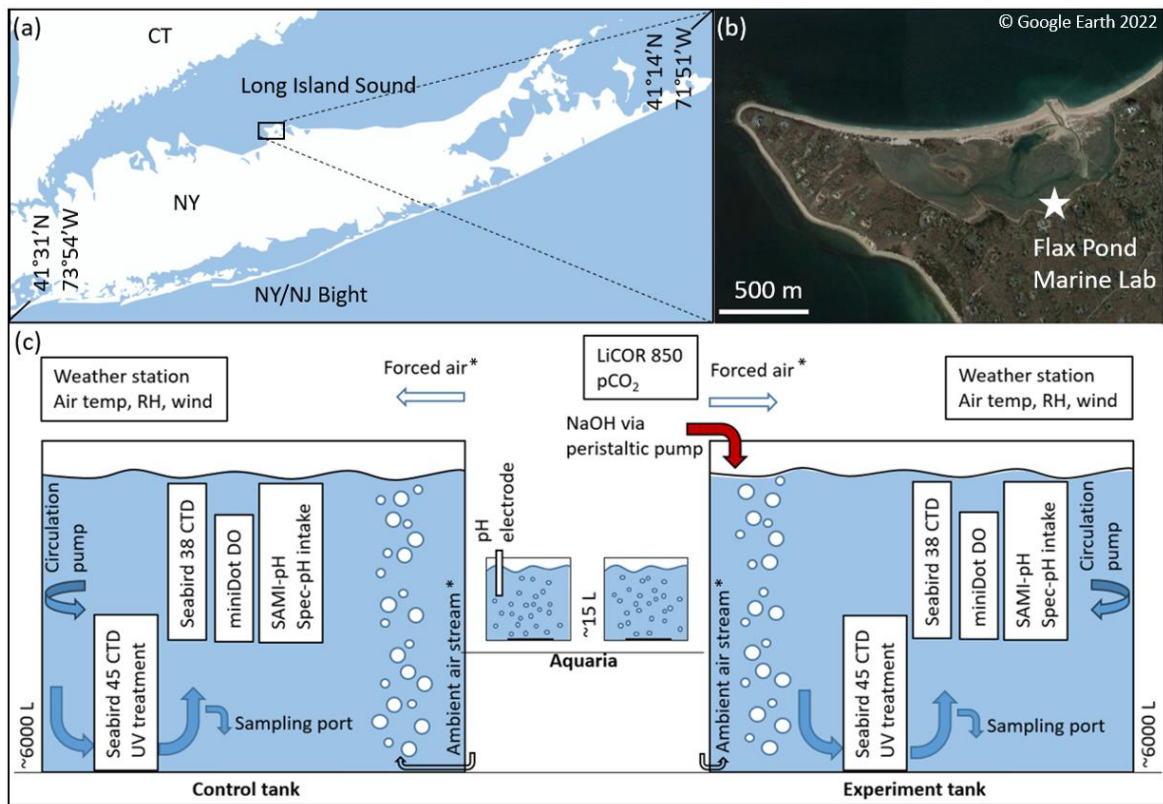
158 (4) What are the threshold values for pH and aragonite saturation state beyond which undesired CaCO<sub>3</sub> precipitation  
159 will occur?

160 Answering these questions is key to assessing the viability of this approach and to optimizing its eventual  
161 deployment. The large tank experiments presented in this manuscript provide a stepping stone between bench-scale  
162 experiments and in-situ mesocosms or field pilots. Even if these experiments simply confirm stoichiometric and  
163 modeled expectations, this is critical information in the design and implementation of OAE deployments. This work  
164 is a necessary part of the growing scientific body that will allow for field trials to progress.

## 165 **2. Methods**

### 166 **2.1 Experimental procedure**

167 We investigated the carbonate chemistry changes resulting from the addition of  $\text{NaOH}_{(\text{aq})}$  to natural seawater over  
 168 timescales ranging from 2 weeks to 2 months in a series of experiments at two scales: (1) two large (~6200 L)  
 169 indoor tanks, and (2) multiple 15 L aquaria (Fig. 1). The large volume of tank experiments allowed for precise  
 170 measurement of the seawater carbonate chemistry via bottle sampling (1L each, sent to NOAA/PMEL for analysis)  
 171 with high sampling frequency. To compliment these measurements, we also performed a series of experiments in  
 172 smaller aquaria (15 L each), which enabled a larger number of replicates and a faster time to equilibrium when  
 173 bubbled with air.



174  
 175 **Figure 1:** (a, b) Flax Pond Marine Laboratory is located on Long Island Sound, New York, USA (© Google Earth  
 176 2022). (c) The ~6000 L control and experiment tanks were instrumented with a series of oceanographic sensors and  
 177 sampled routinely for DIC/ TA analyses to allow for measurement of carbon uptake over time following an addition  
 178 of alkalinity in the form of NaOH. The ~15 L aquaria were instrumented with standard pH electrodes and monitored  
 179 with routine TA analyses. The Forced air\* and Ambient air streams\* indicate their use in some but not all  
 180 experiments, as noted in later sections.

181 This study was conducted at the Flax Pond Marine Laboratory at Stony Brook University, NY. All experiments used  
 182 natural seawater collected from Flax Pond, part of a 128-acre salt marsh tidal wetlands connected to the Long Island  
 183 Sound. The surface areas of the tanks and aquaria were ~4.6 m<sup>2</sup> and ~0.1 m<sup>2</sup>, respectively. The tanks had a diameter  
 184 of 2.4 m, a total height of 1.52 m, and were typically filled to a height of ~1.35 m, allowing for a corresponding  
 185 seawater volume of 6185 L. The aquaria had a diameter of 0.3 m and were typically filled to a height of ~0.23 m, for  
 186 a total seawater volume of 15 L. The large tank volumes were chosen to limit interactions with walls while  
 187 increasing the air-seawater boundary, and to lose a smaller fraction of their volume to evaporation. These tanks  
 188 allow for in-situ oceanographic sensor deployment and frequent bottle sampling while retaining semi-controlled  
 189 temperature, mixing, filtration, and biological control. The inherent limitations of these tank tests include limited air-  
 190 sea interaction, unrealistic light levels and circulation, and biological responses that are not a perfect representation

191 of natural seawater in the ocean, but serve as a stepping stone to mesocosm and eventual field experiments. On  
192 average, the large (~6,000 L) tank experiments took ~6.5 weeks after dosing with NaOH to reach 90% of the  
193 calculated or extrapolated asymptotic  $\Delta\text{DIC}/\text{TA}$  addition ratio indicative of full air-seawater equilibrium, as will be  
194 discussed in Section 3. Therefore, in addition to the large tank tests, we conducted a series of smaller aquaria  
195 alkalinity additions to increase our capacity for experimental test cases. The limitations of the aquaria include  
196 limited sensor options, unrealistic circulation, and limited biological control. While it is expected that equilibration  
197 occurs more rapidly in the small aquaria than in the large tanks, the results from these cases should be similar as  
198  $\text{CO}_2$  equilibrates across the air-sea boundary. However, we note that some variation is expected due to limited  
199 sensing and sampling options in the smaller aquaria and the greater potential for biological growth in the large tanks  
200 over longer timescales.

### 201 **2.1.1 Tank experiments**

202 Seawater was pumped into the tanks at high tide through a series of sock filters to exclude macroscopic biology. The  
203 tanks were then dosed to 40 ppm bleach (sodium hypochlorite) and the shock-treated seawater was allowed to  
204 circulate through the tanks for ~1 day to limit biological growth. The seawater was then circulated through UV light  
205 arrays to break down the bleach over ~1-2 weeks, as assessed by a standard Hach test kit for free chlorine. During  
206 this period, seawater was pumped between the two large test tanks (~25 L/min) to increase mixing of the bleach and  
207 to homogenize the tanks to similar initial conditions. For the remainder of each experiment, the seawater was  
208 continually pumped through the UV sterilizers. Measurements of total alkalinity showed no significant differences  
209 in the bulk seawater TA before and after the bleaching process in any experiment or control tank. In an early  
210 experiment (in which bulk  $\text{pH}_T$  was raised from the initial condition to 8.7, as described below), the initial  $\text{pH}_T$  and  
211 DIC varied between the control and experiment tanks by 0.17 and 77  $\mu\text{mol kg}^{-1}$ , respectively. This was because  
212 seawater was pumped from Flax Pond into multiple reservoirs and was then unevenly distributed between the tanks.  
213 The experiments were subsequently refined to allow for several days of cross-pumping between tanks to  
214 homogenize the control and experiment seawater before NaOH was added at the start of an experiment. More details  
215 on experimental variations and a larger summary table are available in the Supplementary Materials.

216 Oceanographic sensors and discrete daily bottle sampling, as described in Sections 2.2 and 2.3, respectively, were  
217 deployed for carbonate chemistry analysis for several days prior to the alkalinity addition to understand the initial  
218 baseline conditions in both tanks. Two submerged pumps were used for water circulation within each tank: the first  
219 pump (Current eFlux DC Flow Pump, 210 GPH) cycled seawater through the UV arrays with an estimated  
220 overturning time of the bulk tank on order of 1 day, and a second (Kedsum Submersible pump, 260 GPH), mounted  
221 at an angle halfway down the tank wall, allowed for subsurface circulation within the tank to reduce the occurrence  
222 of unmixed ‘dead zones’ and subsequent non-homogenous biological growth, as assessed visually on the surface of  
223 the water and/or tank lining. Initial tank experiments were conducted with a still surface condition, i.e., with no  
224 visible water movement across the surface of each tank. As experiments progressed, forced air movement was added  
225 across the surface of each tank using a stationary fan with a wind speed of ~5 kph. This was done to control for  
226 potential variations in the laboratory HVAC system and to potentially reduce the time to equilibration for the  
227 experiments by increasing the rate of air-sea  $\text{CO}_2$  equilibration. In later experiments, air was bubbled into the bottom  
228 of each tank at a rate of ~30 L  $\text{min}^{-1}$  with an estimated surface area of ~0.3  $\text{m}^2$ , with a goal of further increasing the  
229 rate of equilibration to allow for more rapid throughput of experiments. These variations are further discussed in  
230 Section 2.4.

231 After baselining, one tank (referred to as the “experimental tank”) was dosed with enough 0.5 M NaOH (see  
232 Supplementary Materials) to raise the bulk seawater pH to the target pH of interest for a given experiment, and the  
233 same volume of DI water was added to the other tank (referred to as the “control tank”). NaOH additions were  
234 typically dosed into the tank via peristaltic pump at a low enough rate (~50 mL/min) that a steady increase in bulk  
235 tank pH was observed, but local pH measured just below the NaOH introduction never exceeded a pH of 9.0. A

236 pump (~25 L/min) was placed just below the NaOH stream to speed the mixing of NaOH into the bulk tank,  
237 increase dilution from the point source, and to prevent the immediate precipitation of Mg(OH)<sub>2</sub> upon contact of the  
238 NaOH with seawater. This pump was removed after the full volume of NaOH was mixed into the tank.

239 After the alkalinity addition, the tanks were left to equilibrate with the atmosphere and were monitored by sensors  
240 and sampling as described in Sections 2.2 and 2.3. The tanks were indoors in the wet laboratory at Flax Pond Marine  
241 Lab, such that temperature and CO<sub>2</sub> concentration were moderated by the building's HVAC system, but varied  
242 throughout days and seasons depending on other uses of the lab space. The experiments were concluded when the  
243 observed pH or DIC (calculated from daily pH and frequent TA measurements) appeared to stabilize (e.g., ΔpH  
244 ±0.05% or ΔDIC ±10 μmol kg<sup>-1</sup> per day) over several days. The continuous improvement of experimental methods  
245 during this study resulted in some minor variations among the methods used for each experiment, including methods  
246 of NaOH dosing, tank circulation, and biological control, as discussed where necessary in Section 3 and in the  
247 Supplementary Materials.

## 248 2.1.2 Aquaria experiments

249 A series of polycarbonate aquaria were filled with 15 L of seawater taken from the large control tank just after the  
250 described bleaching and bleach breakdown procedure was completed. NaOH was dosed into each aquarium to reach  
251 a targeted bulk pH<sub>T</sub>, with a corresponding volume of DI H<sub>2</sub>O added to the control aquarium, and then the seawater  
252 was allowed to equilibrate with atmospheric pCO<sub>2</sub> over days to weeks. The aquaria did not have either UV light  
253 arrays for biological control or aquarium pumps for internal circulation. With the exception of a single target pH<sub>T</sub> 8.5  
254 experiment, all aquaria were bubbled with ambient air (~4 L min<sup>-1</sup>) via a standard aquarium bubbling bar spanning  
255 the center diameter of each aquarium, allowing for rapid CO<sub>2</sub> exchange. There was no fine control on air bubbling,  
256 but the surface area of all air bubbles in a given aquarium at any point in time was estimated at ~0.01 m<sup>2</sup>. No sensors  
257 were deployed in the aquaria due to their limited size, and seawater chemistry was established via discrete pH<sub>T</sub> and  
258 TA measurements (Sect. 2.2). An optically clear lid was placed on each aquarium to reduce evaporation and  
259 splashing onto nearby equipment. Some evaporation was evident from the rising TA throughout these experiments,  
260 but was not resolvable within the resolution of a handheld salinometer used for these experiments. Temperature was  
261 discretely recorded from a combination Ross pH electrode.

262 As shown in Eq. (6), we define the dimensionless ‘Carbon-to-Alkalinity Ratio’ (CAR) for our experiments as the  
263 molar ratio of the increase in *n*DIC (in units of μmol/kg, normalized to the system's initial salinity to account for  
264 evaporation) to the magnitude of the TA increase (ΔTA, in units of μmol/kg). *n*DIC<sub>equ</sub> is the measured (via direct  
265 titration) or calculated (via CO2SYS using measured TA and pH<sub>T</sub>) DIC value that the system reached at the end of  
266 an experiment (Pierrot et al., 2006; Van Heuven et al., 2011). Some experiments were left long enough to achieve  
267 equilibration with atmospheric CO<sub>2</sub>, but others were halted early. In these cases, a CO2SYS calculation was used to  
268 estimate the DIC increase expected at equilibration given initial seawater conditions, and the difference between this  
269 value and the final recorded *n*DIC<sub>equ</sub> was used to estimate the overall percent equilibration for a given experiment.  
270 Depending on experimental constraints described in later sections, *n*DIC<sub>i</sub> may represent either: (1) the final *n*DIC  
271 measured (via titration of bottle samples) or calculated (via CO2SYS using seawater TA and pH) in the control tank,  
272 or (2) the ‘baseline’ *n*DIC before the addition of NaOH to a given aquaria experiment, for cases where a  
273 corresponding control case may not be available. Note that because we are reporting CAR values where the  
274 measured DIC has reached or has been estimated at equilibrium, the CAR values we measure and report reflect the  
275 ratio of ΔDIC to ΔTA that would be expected given sufficient time for air-sea exchange to reach equilibrium, and so  
276 are equivalent to directly measuring the value of the “TA addition potential impact ratio” as defined by Wang et al.,  
277 2023.

$$278 \quad \text{Carbon-to-Alkalinity Ratio (CAR)} = (n\text{DIC}_{\text{equ}} - n\text{DIC}_i) / \Delta\text{TA} \quad (6)$$

## 279 2.2 Oceanographic sensors

280 Each tank was instrumented with a series of sensors placed halfway down the wall of the tank near the inlet of the  
281 UV circulation pump. A Seabird 38 Digital Oceanographic Thermometer and Seabird 45 MicroTSG  
282 Thermosalinograph continuously monitored seawater temperature and salinity, respectively. Dissolved oxygen was  
283 measured by a PME miniDOT Logger at 10 min resolution.  $pH_T$  was monitored daily by a SAMI-pH (manufacturer  
284 specified accuracy/precision  $\sim 0.003/0.001$ , though this accuracy is likely an underestimate of the uncertainty given  
285 known challenges for the calibration of the  $pH_T$  measurements) and by a semi-automated spectrophotometric (spec-  
286 pH) pH unit ( $\sim \pm 0.0055/0.0004$ ) as described by Carter et al. (2013). CRM measurements were taken by each pH  
287 system at the beginning and end of each experiment and were used alongside discrete samples of DIC and TA as  
288 described in Section 2.3 to constrain the stability of each sensor. The SAMI-pH measurements were recorded at  
289 ambient seawater temperature and corrected for in-situ salinity as recorded by the Seabird Thermosalinograph  
290 following best practices from the manufacturer. The spec-pH analyses occurred in a jacketed cuvette held at 20 °C  
291 (regulated via water bath) and were corrected to the in-situ bulk tank temperature and salinity as recorded by the  
292 Seabird Thermometer and Thermosalinograph. Both the SAMI-pH and spec-pH rely on spectrophotometric analysis  
293 of metacresol purple indicator dye, which allows for pH measurement within the  $pH_T$  range of approximately 7 to 9.  
294 For experiments in which enough NaOH was dosed into seawater to raise pH above these limits, a Thermo Scientific  
295 Orion ROSS Ultra pH/ATC Triode combination electrode (8157BNUMD) was used to monitor  $pH_{NBS}$  at the surface  
296 of the tank ( $\pm 0.01$  precision), which was then converted to  $pH_T$  for comparison with the other pH sensor systems.

297 A LiCOR LI-850 sensor was used to analyze atmospheric  $pCO_2$  ( $\pm 1.5\%$  accuracy) above the tanks. The inlet to this  
298 sensor was periodically moved between tanks to ensure that atmospheric  $pCO_2$  in the vicinity of the control and  
299 experiment tanks was the same. AcuRite Iris weather stations were mounted on the side of each tank to monitor air  
300 temperature ( $\pm 2$  °C), relative humidity ( $\pm 3\%$ ), and air speed ( $\pm 0.8$  m s<sup>-1</sup>). All data were compiled on an hourly basis  
301 in a custom R package.

## 302 2.3 Discrete sampling

303 Two types of discrete sampling were used to constrain carbonate chemistry throughout these experiments. First, 500  
304 mL of seawater was collected and preserved from each tank, typically on a daily basis, and as frequently as hourly  
305 during the addition of NaOH, following best practices laid out by Dickson (2007) including overflowing of the  
306 sample bottles during collection and addition of 0.2 mL of saturated mercuric chloride (HgCl<sub>2</sub>) as a preservative.  
307 These bottle samples were analyzed for DIC and TA at NOAA Pacific Marine Environmental Laboratory  
308 (NOAA/PMEL). DIC concentrations were measured using a coulometer (UIC Inc.) and Single Operator  
309 Multiparameter Metabolic Analyzer (SOMMA) (Johnson et al., 1985). TA was determined by an open-cell  
310 acidimetric titration (Dickson et al. SOP 3b, 2007). The accuracy of DIC and TA measurements was assessed with  
311 Certified Reference Materials (CRMs, supplied by the Dickson laboratory at Scripps Institution of Oceanography),  
312 and overall uncertainty for both DIC and TA was typically  $\pm 0.1\%$  ( $\sim 2$   $\mu\text{mol/kg}$ ).

313 In addition, discrete seawater samples were analyzed for TA via open-cell potentiometric titration at Stony Brook  
314 University. A Thermo Scientific Orion ROSS Ultra pH/ATC Triode combination electrode (8157BNUMD),  
315 calibrated using three buffer solutions ( $pH_{NBS}$  4.01, 7, and 10.01) was used to track the titration of a  $\sim 20$  mL  
316 seawater sample with a dilute HCl solution ( $\sim 0.1$  M in 0.7 M NaCl, calibrated daily with CRM or a secondary  
317 seawater standard) following a modified Gran titration procedure using a Klotz digital syringe pump (Song et al.,  
318 2020; Wang and Cai, 2004). The precision of TA measurements was  $\sim \pm 5$ -10  $\mu\text{mol/kg}$ . This TA data was corrected  
319 to that of the bottle samples analyzed via titration at NOAA PMEL where available (see Supplementary Materials).

320 There are several differences between the aquaria experiments and the larger tank experiments. First, the aquaria  
321 experiments were monitored daily to every few days by discrete measurement of TA at Stony Brook University and



322  $\text{pH}_{\text{NBS}}$  via Thermo Scientific Orion ROSS Ultra pH/ATC Triode combination electrode (8157BNUMD) ( $\pm 0.01$   
323 precision), which was then converted to  $\text{pH}_{\text{T}}$  and corrected against the other pH sensor systems via occasional bottle  
324 samples for DIC and TA analysis at NOAA PMEL. Variations between these experiments are noted in Section 3  
325 where necessary and in the Supplementary Materials.

326 In either tank or aquaria cases where mineral precipitation was observed, 0.5 – 1 L of seawater was vacuum filtered  
327 through a 0.45  $\mu\text{m}$  Whatman GF/F filter via vacuum pump and the solids were rinsed with DI water 3 times to  
328 remove NaCl. The precipitate was dried in an oven at 90 °C, then crushed into a uniform powder via mortar and  
329 pestle. Samples were analyzed via Hitachi 4800 Scanning Electron Microscopy (SEM) (5 kV) and Rigaku SmartLab  
330 X-ray Diffraction (XRD) (Cu  $\text{K}\alpha$ , 1.5406 Å, 10 - 100° 2  $\theta$  at 4°/min) at Brookhaven National Laboratory at the  
331 Materials Synthesis and Characterization Facility of the Center for Functional Nanomaterials.

## 332 **2.4 Evaluation of CO<sub>2</sub> uptake by seawater in response to NaOH perturbation**

333 Seawater carbonate chemistry measurements were used to analyze the uptake of CO<sub>2</sub> in each tank, primarily relying  
334 on calculations from the NOAA/PMEL DIC and TA analyses of bottle samples when available and using sensor pH  
335 and Stony Brook TA measurements for cross-verification or to fill in between discrete DIC samples. DIC and TA  
336 data were normalized to the salinity at the start of a given experiment to account for evaporation (Friis et al., 2003).  
337 Carbonate chemistry calculations were then performed using CO2SYS (Lewis and Wallace, 1998), with Lueker et  
338 al. (2000) carbonate constants, Dickson (1990) for KSO<sub>4</sub>, and Lee et al. (2010) for total boron. Wherever possible, a  
339 combination of CRM analyses and comparisons between simultaneous pH sensor and NOAA PMEL bottle samples  
340 were used to correct SAMI-pH and spectrophotometric pH sensor data for drift.

341 Changes in the seawater carbonate chemistry over time were analyzed with respect to shifts away from the baseline  
342 within a single control or experiment tank, as well as with respect to the differences between the control and  
343 experimental tanks.

## 344 **3 Results and Discussion**

### 345 **3.1 Large tank experiments**

346 A summary of the range of oceanographic variables measured by sensors and bottle samples, calculated via  
347 CO2SYS, or extrapolated to equilibration conditions during the large tank experiments is provided in Table 1. This  
348 summary includes 6 experiments including 3 targeting  $\text{pH}_{\text{T}}$  8.5 (still surface water, with forced air, and with forced  
349 air and air bubbling) and one (each) targeting  $\text{pH}_{\text{T}}$  values of 8.7 (still surface water), 9.5 (with forced air and air  
350 bubbling), and 10.3 (still surface water). While the initial seawater conditions were similar between the control and  
351 experiment tanks, we note that these cases are not entirely comparable after the termination of cross-pumping  
352 between tanks and the subsequent addition of alkalinity. While tanks were initially bleached, eventually some  
353 biological growth was noted in each tank with potential differences in spatial and temporal distribution as well as  
354 species and community differences. Herein, we assume that differences between the control and experiment cases  
355 are due to the addition of alkalinity alone, but we note that characterization of other potential confounding factors is  
356 a subject for future work.

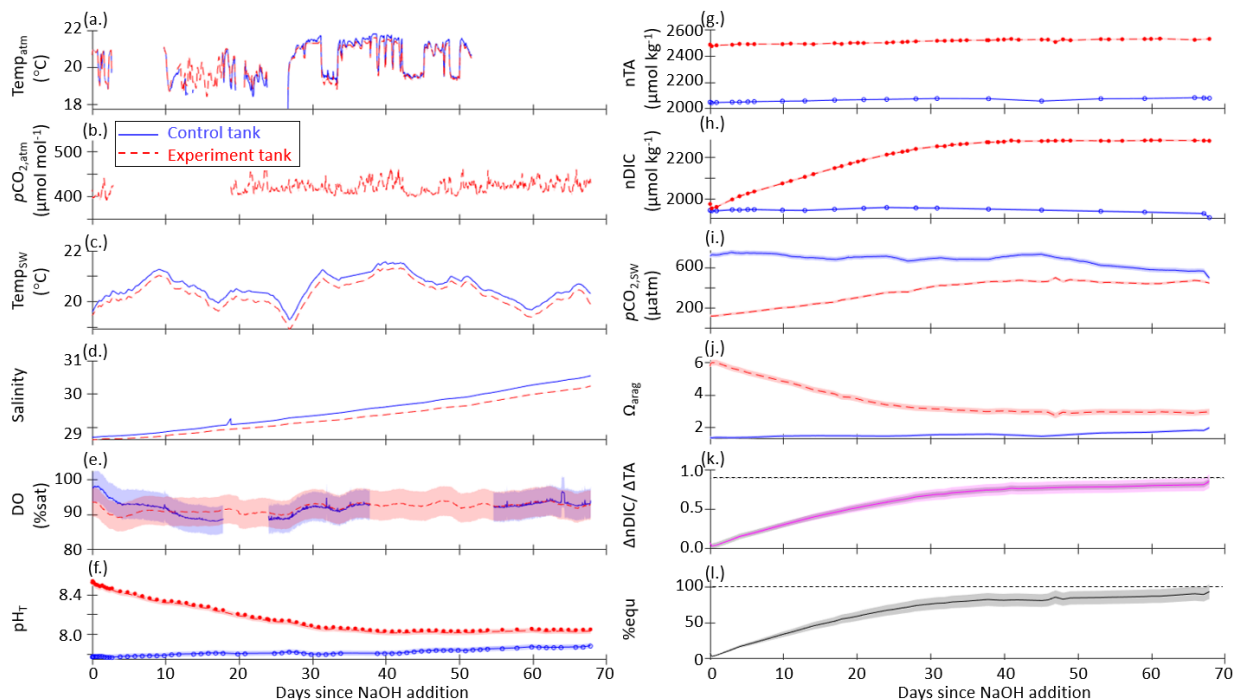
357 The initial  $\text{pH}_{\text{T}}$ , TA, and DIC varied across experiments as seawater was collected between March 2022 and May  
358 2023, ranging from pH 7.66 (December 2022) – 7.95 (May 2023), TA 2001 (May 2023) – 2176 (March 2023)  
359  $\mu\text{mol/kg}$ , and DIC 1847 (May 2023) – 2021 (March 2023)  $\mu\text{mol/kg}$ . Both measured and CO2SYS -calculated DIC  
360 and TA values were normalized to salinity to account for evaporation, which drove salinity increases ranging from  
361 0.2 – 7.1 across these experiments.

362 After the addition of NaOH, the control and experiment tanks were allowed to equilibrate with atmospheric CO<sub>2</sub>.  
 363 While refinements in the experimental design allowed for complete or near-complete equilibration in later  
 364 experiments, as determined by the stabilization of nDIC at some asymptotic value, early experiments were  
 365 terminated before full equilibration. In all experiments, the absorption of atmospheric CO<sub>2</sub> began immediately after  
 366 the NaOH addition, as determined by decreasing pH and  $\Omega_{\text{arag}}$  and increasing DIC and seawater pCO<sub>2</sub>. nTA was  
 367 fairly stable or increasing (+10 - 60  $\mu\text{mol kg}^{-1}$ ) after the NaOH addition in all cases except the pH<sub>T</sub> = 10.3  
 368 experiment, where nTA and DIC rapidly decreased due to runaway CaCO<sub>3</sub> precipitation. A stable TA value is an  
 369 indicator that no significant persistent mineral precipitation (e.g., Mg(OH)<sub>2</sub> or CaCO<sub>3</sub>) has occurred. In the absence  
 370 of active mixing or bubbling, Mg(OH)<sub>2</sub> precipitation occurred immediately upon the introduction of NaOH to  
 371 seawater, however the precipitation can be rapidly dissolved by turbulence (i.e., pumping NaOH directly above a  
 372 strong circulation pump and/or stream of air bubbles). No CaCO<sub>3</sub> precipitation was observed in the tanks or aquaria  
 373 for which the bulk seawater pH<sub>T</sub> was <10.0. The pH<sub>T</sub> = 10.3 experiment was designed to induce CaCO<sub>3</sub> runaway  
 374 precipitation, as described in Section 3.3.

375  $\Omega_{\text{arag}}$  ranged from 1.4 - 2.5 in the control tanks with minimal variation over the course of any given experiment.  
 376 During the three experiments in which bulk pH<sub>T</sub> was increased to ~8.5,  $\Omega_{\text{arag}}$  increased immediately to 6.0 - 6.3 at the  
 377 peak of the experiments, before slowly decreasing to 2.8 - 3.0 as the seawater equilibrated with atmospheric CO<sub>2</sub>.  
 378 For the bulk pH<sub>T</sub> 9.5 experiment,  $\Omega_{\text{arag}}$  increased to 20.2 and slowly decreased to 5.0 when the experiment was  
 379 ended at full equilibration. Mineral precipitation was observed in the bulk pH<sub>T</sub> 10.3 experiment, where  $\Omega_{\text{arag}}$  was  
 380 increased to 30.3 and rapidly (<1 week) fell to 5.2 after the addition of NaOH.

381 The results of one representative set of time-series measurements from the control and experiment tanks are shown  
 382 in Figure 2 for the case where pH<sub>T</sub> of the bulk experiment tank was raised to 8.5 then allowed to relax into  
 383 equilibration with the atmosphere without the addition of surface air forcing or bubbling. Time-series plots for the  
 384 other tank-scale experiments are available in the Supplementary Materials.

385



386

387 **Figure 2:** Time-series data for the case where  $\text{pH}_T$  of the bulk experiment tank was raised to 8.5 with no forced air  
388 flow and no bubbling (still surface) for control (blue, solid) and experiment (red, dashed) tanks: (a) continuously  
389 measured air temperature, (b) atmospheric  $p\text{CO}_2$ , (c) seawater temperature, (d) salinity, and (e) dissolved oxygen; (f)  
390  $\text{pH}_T$  measured by the SAMI-pH (*circles*) and interpolated from the spec-pH (*line*), corrected to bottle sample and  
391 CRM data; (g) NOAA/PMEL-measured TA and (h) DIC from bottle samples and normalized to salinity; (i)  
392 seawater  $p\text{CO}_2$  and (j) saturation state of aragonite ( $\Omega_{\text{arag}}$ ) calculated from interpolated  $n\text{DIC}$  and  $n\text{TA}$  data via  
393 CO2SYS; (k) the observed carbon uptake ratio (CAR) as  $(n\text{DIC}_{\text{exp}} - n\text{DIC}_{\text{control}}) / \Delta\text{TA}_{\text{NaOH addition}}$  (*solid*) and the  
394 theoretical CAR (*dashed*) from a CO2SYS calculation using measured TA and the average  $p\text{CO}_{2,\text{atm}}$  to estimate the  
395 equilibrium change in DIC (*dashed*); (l) the percent equilibration estimated between the observed and theoretical  
396 CAR. Data gaps in panels a, b, and e are due to connectivity issues while offloading sensor data.

397 The  $\Delta n\text{TA}$  and  $\Delta n\text{DIC}$  values calculated between the control and experiment tanks are summarized in Figure 3  
398 where  $n\text{TA}$  and  $n\text{DIC}$  were interpolated between bottle samples measured at NOAA-PMEL, and/or were calculated  
399 via CO2SYS using sensor  $\text{pH}_T$  and TA measured at Stony Brook University corrected to less frequent NOAA-  
400 PMEL TA and DIC bottle samples. The ratio of the  $\Delta n\text{DIC}$  to the addition of alkalinity in the form of NaOH, or  
401  $\Delta n\text{TA}$ , is included in Figure 3 for all experiments except that of the bulk  $\text{pH}_T$  increase to 10.3. Neglecting  
402 experiments that were terminated before full equilibration, the final observed CAR ranged from  $0.75 \pm 0.04$  to  $0.87$   
403  $\pm 0.08$  (Table 1).

404 An anomalous event was noted in both the experiment and control cases for the target  $\text{pH}_T$  8.5 experiment with  
405 forced air movement across the surface of the tank, wherein an increase in TA and DIC was noted around day 30 of  
406 the experiment. The cause of this event is unclear but could include biological changes in both tanks, the  
407 introduction of alkalinity from environmental contaminants, or the anomalous delayed release of alkalinity from  
408 suspended solids. This event was not observed in any other case, and highlights the importance of using controls to  
409 understand complex interactions in these experiments. A time-series including this event is available in the  
410 Supplementary Materials.

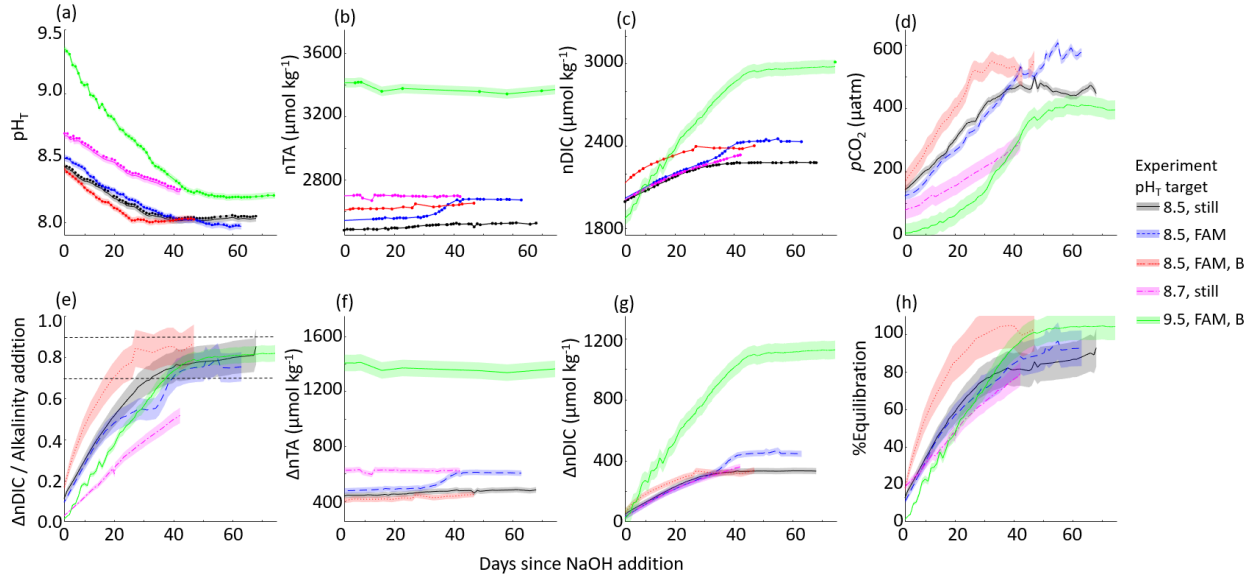
411 Henry's law and CO2SYS calculations were used to estimate the initial and final equilibration condition of each  
412 tank experiment. LiCOR  $p\text{CO}_{2,\text{atm}}$  measurements were averaged across experiments to a representative value of  $421$   
413  $\pm 14$  ppm, which was used with the initial seawater temperature and salinity to estimate  $p\text{CO}_{2,\text{seawater}}$  at the beginning  
414 of each experiment. This initial  $p\text{CO}_{2,\text{seawater}}$  was in all cases greater than the atmospheric  $p\text{CO}_{2,\text{seawater}}$ , indicating  
415 that the seawater was not fully equilibrated with the atmosphere at the time when NaOH was added, likely due to  
416 respiration and decomposition of organic material (Section 2.1), and as such, the tanks should outgas  $\text{CO}_2$ . The  
417 initial equilibrium DIC was estimated from a CO2SYS calculation using the  $p\text{CO}_{2,\text{seawater}}$  and  $n\text{TA}_i$ , which in all  
418 cases was less than the initial  $n\text{DIC}$  measured or calculated from  $n\text{TA}_i$  and  $\text{pH}_{T,i}$  (by  $29 - 108 \mu\text{mol kg}^{-1}$ ). These  
419 observations underscore the importance of having a control tank to capture natural dynamics of  $\text{CO}_2$  ingassing and  
420 outgassing to ensure that changes in DIC attributed to OAE are correctly accounted for.

421 The final equilibrium  $n\text{DIC}$  was estimated from a CO2SYS calculation using the same  $p\text{CO}_{2,\text{seawater}}$  and the  $n\text{TA}$   
422 measured just after the NaOH addition, corrected for the linear increase in salinity over the course of the experiment.  
423 The ratio of the expected  $\Delta n\text{DIC}$  calculated at equilibrium with the atmosphere to the addition of alkalinity provides  
424 a simple estimate of the expected  $\text{CO}_2$  storage capacity for a given experiment. The percent equilibration for each  
425 experiment was then estimated from the measured and expected values for CAR. Within the series of experiments  
426 with a targeted  $\text{pH}_T$  of 8.5, the timeline to reach an estimated 90%  $\text{CO}_2$  equilibration decreased from 65 days (with  
427 internal circulation but still water at the surface of the tank), to 50 days (with the addition of forced air movement  
428 across the surface of the tank) to 22 days (with the addition of air bubbling). We note that only the two cases  
429 (targeted  $\text{pH}_T$  of 8.5 and 9.5) with the addition of air bubbling reached full equilibration with the atmosphere.

430 **Table 1:** Range of variables measured, calculated, or extrapolated in large tank experiments, where M denotes direct  
 431 measurement, C denotes calculation via CO2SYS, and E denotes extrapolation to equilibrium conditions. Subscripts  
 432 *i* and *f* refer to initial and final conditions, and ‘peak’ refers to the time point immediately after the addition of  
 433 NaOH.

pH target	-	8.5		8.5		8.5		8.7		9.5		10.3	
Surface condition	-	Still		Forced Air		Forced Air and Air Bubbles		Still		Forced Air and Air Bubbles		Still	
Tank (C = control, E = experiment)	-	C	E	C	E	C	E	C	E	C	E	C	E
$\Delta TA = \text{NaOH addition } (\pm 10 \mu\text{mol/kg})$	M	0	409	0	462	0	375	0	626	0	1406	0	3305
Salinity <sub>i</sub> (g/kg)	M	28.7	28.7	30.2	30.2	30.4	30.4	26.9	26.8	26.9	26.9	28.5	28.4
Salinity <sub>f</sub> (g/kg)	M	30.5	30.2	37.3	36.6	34.7	33.7	27.6	27.6	29.0	29.2	28.6	28.6
pH <sub>T,i</sub> ( $\pm 0.005$ )	M	7.76	7.76	7.73	7.73	7.93	7.93	7.92	7.75	7.95	7.95	7.70	7.75
pH <sub>T,peak</sub> ( $\pm 0.005$ )	M	-	8.54	-	8.58	-	8.49	-	8.68	-	9.51	-	10.10
pH <sub>T,f</sub> ( $\pm 0.005$ )	M	7.88	8.05	7.85	7.99	7.99	8.01	7.84	8.26	8.01	8.21	7.75	9.52
$nTA_i$ ( $\pm 10 \mu\text{mol/kg}$ )	M	2049	2049	2069	2069	2248	2248	2075	2075	2007	2007	2023	2025
$nTA_{\text{peak}}$ ( $\pm 10 \mu\text{mol/kg}$ )	M	-	2458	-	2531	-	2623	-	2701	-	3414	-	5330
$nTA_f$ ( $\pm 10 \mu\text{mol/kg}$ )	M	2080	2528	2235	2674	2246	2624	2095	2696	2014	3363	2041	1253
$nDIC_i$ ( $\mu\text{mol/kg}$ )	M	1944	1947	1957	1996	2082	2087	1897	1975	1852	1852	1928	1938
$nDIC_f$ ( $\mu\text{mol/kg}$ )	M	1908	2280	2084	2433	2027	2365	1937	2336	1832	2977	1947	720
$\Omega_{\text{aragonite},i}$	C	1.39	1.37	1.4	1.1	2.0	2.0	2.4	2.4	1.9	1.9	1.4	1.3
$\Omega_{\text{aragonite,peak}}$	C	-	5.9	-	6.0	-	6.2	-	8.8	-	19.3	-	30.3
$\Omega_{\text{aragonite},f}$	C	2.0	3.0	1.7	2.8	2.5	3.0	1.9	4.4	2.1	4.9	1.4	5.2
CAR <sub>f</sub>	C	-	$0.85 \pm 0.04$	-	$0.75 \pm 0.04$	-	$0.87 \pm 0.08$	-	$0.52 \pm 0.07$	-	$0.82 \pm 0.09$	-	-
CAR <sub>equilibrium</sub>	E	-	0.89	-	0.85	-	0.85	-	0.84	-	0.81	-	-
% equilibration (time elapsed in days)	E	-	$95 \pm 10$ (67)	-	$92 \pm 10$ (63)	-	$102 \pm 12$ (45)	-	$79 \pm 6$ (42)	-	$104 \pm 7$ (74)	-	(13)

434



435

436 **Figure 3:** Results of 5 tank-scale experiments in which enough NaOH was added to each tank to raise the bulk pH<sub>T</sub>  
 437 to 8.3 – 9.7. pH<sub>T</sub> decreased rapidly in all cases in which air bubbling sped equilibration with atmospheric CO<sub>2</sub>.  
 438 Results include: (a) measured pH<sub>T</sub>, (b) measured nTA, (c) measured nDIC or CO<sub>2</sub>SYS calculated (for pH<sub>T</sub> 9.5 case  
 439 only), (d) CO<sub>2</sub>SYS -calculated pCO<sub>2</sub>, (e) the observed carbon uptake ratio (CAR) as (nDIC<sub>exp</sub> - nDIC<sub>control</sub>) /  
 440 ΔnTA<sub>NaOH addition</sub> with horizontal dashed lines representing the expected range of 0.7-0.9 mol CO<sub>2</sub> uptake / mol NaOH  
 441 added to seawater, the change in (f) nTA and (g) nDIC compared to the baseline measurements before the addition  
 442 of NaOH, and the percent equilibration estimated between the observed and theoretical CAR.

443 **3.2 Aquaria experiments**

444 Table 2 provides a summary of the range of oceanographic variables quantified for the aquaria experiments.

445 **Table 2:** Range of variables measured, calculated, or extrapolated in aquaria experiments, where M denotes direct  
 446 measurement, C denotes calculation via CO<sub>2</sub>SYS, and E denotes estimation within specified equilibration  
 447 conditions. Subscripts *i* and *f* refer to initial and final conditions, and ‘peak’ refers to the time point immediately  
 448 after the addition of NaOH.

pH target	-	0 Control	8.3	8.5	8.5 Without air bubbles	8.7	9.3	9.5	9.7	9.9	10.0	10.1	10.2	10.3
ΔTA = NaOH addition (± 10 μmol/kg)	M	0	187	331	362	543	1409	1679	2037	2216	2276	2504	2796	3829
pH <sub>T,i</sub> (± 0.1)	M	7.94	7.97	7.90	7.86	7.95	7.98	7.98	7.98	8.06	8.04	8.04	8.04	7.95
pH <sub>T,peak</sub> (± 0.1)	M	-	8.28	8.41	8.40	8.63	9.22	9.43	9.64	9.83	9.91	10.23	10.32	10.20
pH <sub>T,f</sub> (± 0.1)	M	8.06	8.03	8.07	8.11	8.08	8.21	8.20	8.23	8.65	8.96	8.72	9.46	7.99
TA <sub>i</sub> (± 10 μmol/kg)	M	2265	2262	2250	2250	2250	2393	2393	2393	2531	2531	2531	2531	2250
TA <sub>peak</sub> (± 10 μmol/kg)	M	-	2449	2582	2611	2793	3801	4072	4430	4748	-	-	-	4608
TA <sub>f</sub> (± 10 μmol/kg)	M	2323	2476	2640	2645	2822	3837	4110	4420	4462	1702	1835	1537	2202
DIC <sub>i</sub> (μmol/kg)	C	2089	2073	2091	2107	2070	2192	2192	2192	2282	2287	2287	2287	2067

DIC <sub>f</sub> (μmol/kg)	C	2113	2246	2377	2382	2540	3372	3486	3877	3389	992	1244	671	2003
Ω <sub>aragonite,i</sub>	C	2.1	2.2	1.9	1.8	2.1	2.34	2.4	2.4	2.9	2.8	2.8	2.8	2.1
Ω <sub>aragonite,peak</sub>	C	-	4.2	5.5	5.5	8.1	19.5	23.1	27.0	29.8	30.2	30.9	32.4	38.9
Ω <sub>aragonite,f</sub>	C	2.4	2.7	3.1	3.1	3.4	5.9	7.9	7.1	13.7	6.5	5.7	7.0	2.2
CAR <sub>f</sub>	C	-	0.92 ± 0.10	0.87 ± 0.06	0.76 ± 0.05	0.87 ± 0.04	0.84 ± 0.02	0.86 ± 0.02	0.84 ± 0.02	0.50	-	-	-	-
CAR <sub>equilibrium</sub>	E	-	0.69	0.67	0.64	0.77	0.80	0.80	0.80	0.81	-	-	-	-
% equilibration (time elapsed in days)	E	(40)	130 (16)	126 (18)	116 (40)	111 (16)	104 (18)	106 (18)	104 (18)	62 (1)	(1)	(1)	(1)	(16)
CaCO <sub>3</sub> precipitation?	M	-	No	No	No	No	No	No	No	No	Yes	Yes	Yes	Yes

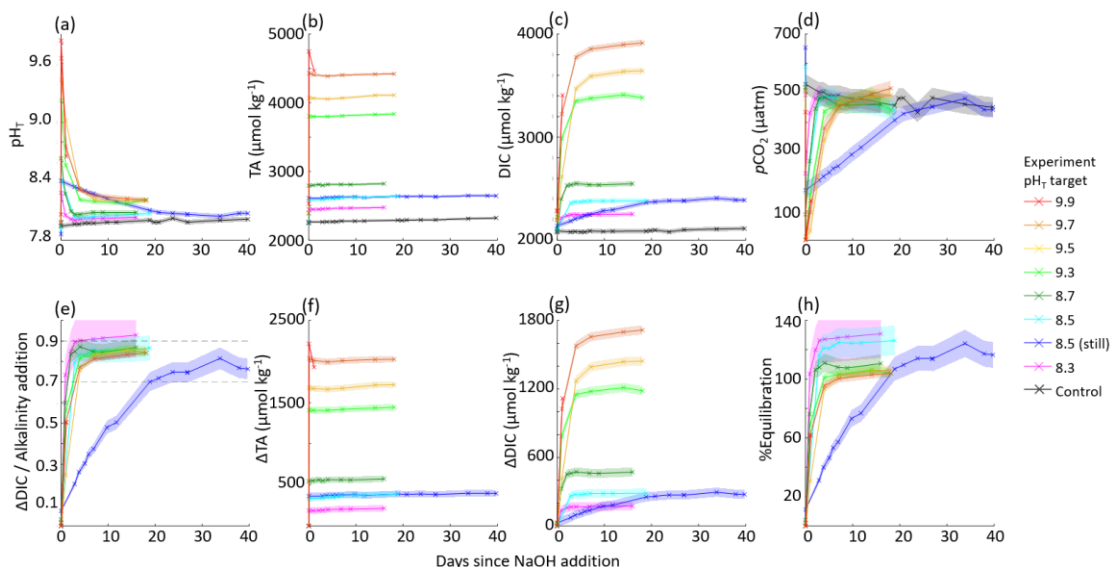
449 The aquaria experiments are not directly comparable to the control stated in Table 2. Seawater for one control  
450 aquarium was collected in March 2023, and was monitored for pH<sub>T</sub> and TA changes through May 2023. Seawater  
451 for the experimental aquaria was collected in three batches between March, April, and May 2023, with only 4-6  
452 aquaria experiments running in parallel within each set of experiments due to space and analytical throughput  
453 constraints. Because of this, the experiments started in March 2023 could be compared directly to the control (target  
454 pHT 8.3, 8.5, 8.5 still, and 8.7), but the rest of the experiments used different initial seawater than the control  
455 aquarium. The CAR for each aquaria experiment was therefore calculated from changes in DIC and TA between the  
456 initial ‘baseline’ condition and after the NaOH was added within a given aquarium, rather than between the  
457 experiment and control cases. The CAR ranged between 0.76 ± 0.05 and 0.92 ± 0.10, excluding cases where mineral  
458 precipitation was evident and for the pH<sub>T</sub> 9.9 case where the experiment ended after one day due to a sensor logging  
459 failure. This wide range in ΔDIC/ ΔTA is likely due to the limited number of TA samples collected throughout these  
460 experiments (daily at best with no duplicates due to the limited volume), and the imprecision of electrode-based pH<sub>T</sub>  
461 measurements relative to the SAMI-pH and spec-pH based measurements used in the large tank experiments.

462 No significant changes in salinity were recorded during these experiments as measured by a handheld salinometer  
463 with a range of 30 - 31. Therefore, DIC and TA were not normalized to salinity. Temperature values ranged from 19  
464 - 21 °C during the experiments.

465 Similar to the large tank experiments, we used Henry’s law and CO2SYS calculations to estimate the initial and  
466 final equilibration condition of each aquaria experiment. The same average pCO<sub>2,atm</sub> of 421 ± 14 ppm was used with  
467 the initial seawater temperature and salinity to estimate pCO<sub>2,seawater</sub> at the beginning of each experiment. The initial  
468 equilibrium DIC was estimated from a CO2SYS calculation using this pCO<sub>2,seawater</sub> and TA<sub>i</sub>, which in all cases was  
469 less than the initial DIC calculated from TA<sub>i</sub> and pH<sub>T,i</sub> (by 16 – 36 μmol kg<sup>-1</sup>). This indicates that the seawater was  
470 not fully equilibrated with the atmosphere at the time when NaOH was added, likely due to respiration and  
471 decomposition of organic material (Section 2.1), and as such, the aquaria should outgas CO<sub>2</sub>. The final equilibrium  
472 DIC was estimated from a CO2SYS calculation using the same pCO<sub>2,seawater</sub> and the TA measured just after the  
473 NaOH addition. The percent equilibration for each experiment was then estimated between the measured and  
474 predicted values for ΔDIC/ ΔTA. Due to the air bubbling, most experiments approached equilibrium with the  
475 atmosphere within 1-7 days, with the exception of the non-bubbled pH<sub>T</sub> 8.5 experiment that took ~20 days. The  
476 surface water of this non-bubbled experiment was stagnant, and the water was only mixed via stirring just before  
477 taking pH and TA samples. Absorption of atmospheric CO<sub>2</sub> began immediately after the NaOH addition, as  
478 determined by decreasing pH<sub>T</sub>. We note that there are significant uncertainties in these equilibrium estimates leading  
479 to estimates of >100% equilibration. These estimates would be better constrained with more continuous carbonate  
480 chemistry measurements, particularly seawater and atmosphere pCO<sub>2</sub> throughout the experiments that would allow  
481 for more direct calculation of air-sea CO<sub>2</sub> flux and equilibration, and finer control of bubbling and diffusion rates are  
482 necessary to define the timeline for equilibration within the aquaria.

483 Each aquaria was gently stirred during the addition of NaOH to prevent and/or redissolve  $Mg(OH)_2$  precipitation.  
 484 No  $CaCO_3$  precipitation was observed in the tanks below a bulk seawater  $pH_T$  of 10.0, and TA remained stable in  
 485 each of these experiments with the exception of some increase driven by minor evaporation on the order of +2  
 486  $\mu\text{mol/kg}$  per day. Experiments where  $CaCO_3$  precipitation was induced by increasing the starting  $pH$  to values above  
 487 10 are discussed in Section 3.3.

488 The aquaria experiments with target  $pH_T$  from 8.3 – 9.9 are summarized in Figure 4.

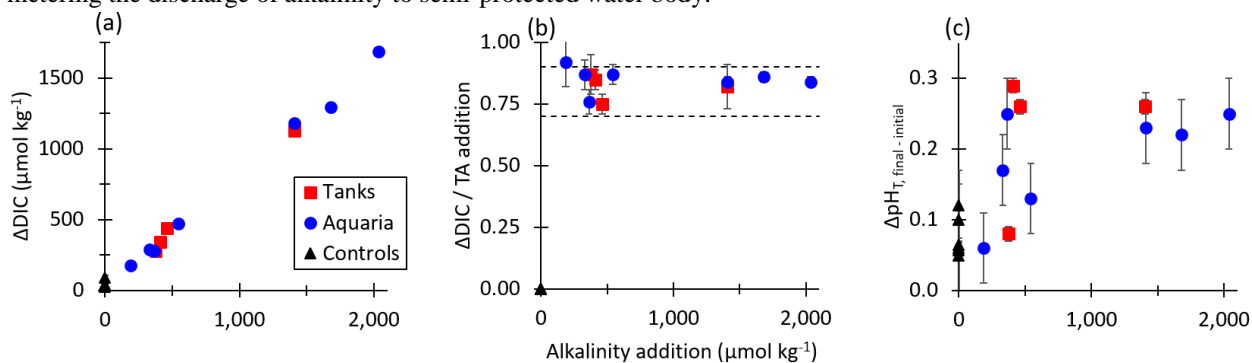


489  
 490 **Figure 4:** Results of 9 aquaria experiments in which enough NaOH was added to each aquaria to raise the bulk  $pH_T$   
 491 to 8.3 – 9.9.  $pH_T$  decreased rapidly in all cases in which air bubbling sped equilibration with atmospheric  $CO_2$ .  
 492 Results include: (a) measured  $pH_T$ , (b) measured TA, (c) CO2SYS-calculated DIC, (d) CO2SYS-calculated  $pCO_2$ ,  
 493 (e) the observed carbon uptake ratio (CAR) as  $(DIC_{exp} - DIC_{baseline}) / \Delta TA_{NaOH\ addition}$  with horizontal dashed lines  
 494 representing the expected range of 0.7-0.9 mol  $CO_2$  uptake / mol NaOH added to seawater, the change in (f) TA and  
 495 (g) DIC compared to the baseline measurements before the addition of NaOH, and the percent equilibration  
 496 estimated between the observed and theoretical CAR.

497 In general, the large tanks and aquaria showed reasonable agreement in achieving values for CAR within the  
 498 expected range of 0.7-0.9 (He and Tyka, 2023; Burt et al., 2021; Wang et al., 2023). While the use of aquaria  
 499 bubbled with air to speed equilibration allowed for a greater range of data collection within a constrained experiment  
 500 timeline, the quality of this data is limited by the lack of appropriate sensors to fit into these small 15 L aquaria and  
 501 fewer bottle samples due to the reduced quantity of seawater. However, while the large tanks allow for a larger  
 502 range of oceanographic sampling and sensing techniques, it is more challenging to fully quantify mixing and  
 503 circulation rates in the current large tank experimental setup.

504 Figure 5 shows the dependence of the equilibrium values of  $\Delta DIC$ , CAR, and  $\Delta pH_T = (pH_{final} - pH_{initial})$  as a function  
 505 of the alkalinity addition for both tank and aquaria experiments in which the final percent equilibration for  $CO_2$  was  
 506 estimated at greater than 90%. Results for tank and aquaria experiments aligned well, with increasing  $\Delta DIC$  for  
 507 increasing alkalinity additions. The CAR was observed for all experiments to fall within the range expected for  
 508 seawater with the temperature and salinity values used in these tests. As expected from calculations of the response  
 509 of the seawater carbonate buffer system to additions of alkalinity, the  $pH_T$  at equilibrium exceeded the initial  $pH_T$   
 510 value prior to the addition of alkalinity. That is, even once equilibrium in the alkalinity enhanced experiment tank  
 511 had been reached, the ending  $pH$  value was slightly elevated relative to the starting  $pH$  value. This finding warrants

512 further investigation on the potential of OAE to mitigate some acidification impacts in controlled field trials by  
513 metering the discharge of alkalinity to semi-protected water body.



514 **Figure 5:** (a) The change in final CO2SYS-predicted DIC relative to the initial conditions for tank, aquaria, and  
515 control experiments increases with increasing NaOH additions for cases where the air-sea CO<sub>2</sub> equilibration was  
516 estimated at >90% at the termination of each experiment. (b) CO2SYS-predicted CAR ( $\Delta\text{DIC} / \text{Alkalinity addition}$ )  
517 at air-sea equilibrium conditions for tank, aquaria, and control experiments, with horizontal dashed lines  
518 representing the expected range of 0.7-0.9 mol CO<sub>2</sub> uptake / mol NaOH added to seawater. (c) The measured  $\Delta\text{pH}_{\text{T}}$   
519  $= (\text{pH}_{\text{final}} - \text{pH}_{\text{initial}})$  increases with  
520

521 alkalinity addition for both tank and aquaria experiments.

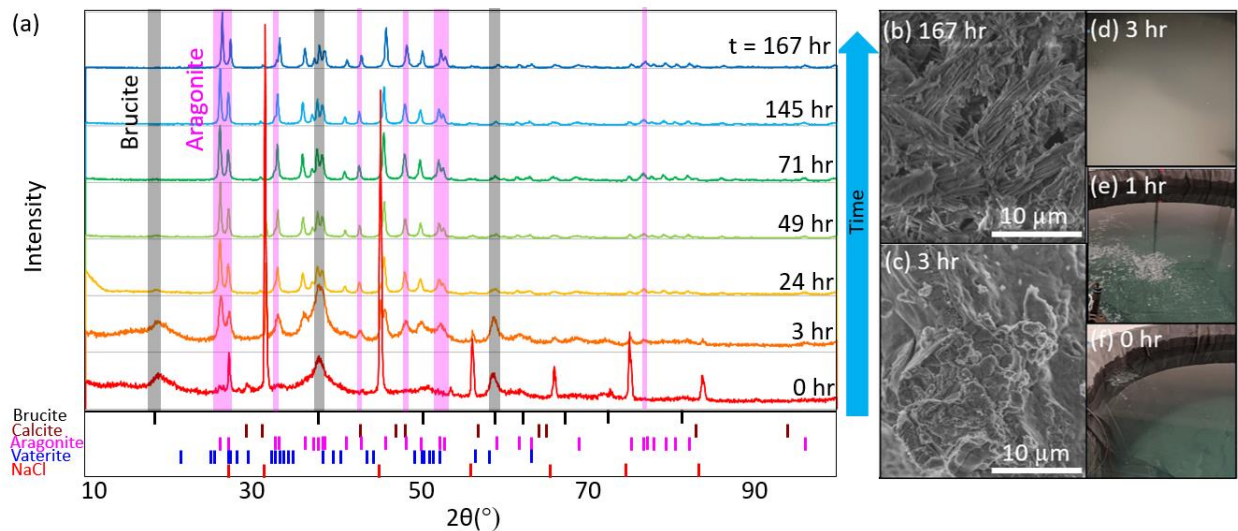
### 522 3.3 Experiments exceeding the CaCO<sub>3</sub> precipitation threshold

523 While Mg(OH)<sub>2</sub> precipitation occurs immediately upon introduction of concentrated (i.e., ~0.5 M) NaOH to still  
524 seawater, it may be rapidly dissolved or avoided entirely by gentle mixing, including via the use of stirrers,  
525 circulation pumps, or air bubblers. This precipitation and redissolution happened rapidly enough that it was not  
526 identified in any TA or other variables measured in the aquaria and tank tests. However, in cases where enough  
527 NaOH was added to raise the bulk seawater pH<sub>T</sub> to greater than 10.0 (i.e. in one large tank test with a target pH<sub>T</sub> of  
528 10.3, and in 4 aquaria experiments ranging from pH<sub>T</sub> 10.0-10.3), runaway precipitation of Mg(OH)<sub>2</sub> and CaCO<sub>3</sub> was  
529 observed. This was characterized by a sharp reduction in both TA and DIC and an increase in turbidity. Runaway  
530 precipitation has been described as a condition in which more alkalinity is removed from seawater by mineral  
531 precipitation than was initially added until a new steady state is achieved (Moras et al., 2022; Hartmann et al., 2023;  
532 Suitner et al., 2023). This can significantly impact the efficiency of OAE, and has implications for biological  
533 productivity, as increased turbidity may impact photosynthesis or predator-prey interactions.

534 In both the tank and aquarium pH<sub>T</sub> 10.3 cases, discrete samples of the precipitate were collected at seven different  
535 times after the bulk pH<sub>T</sub> value reached 10.3 (0h, 3h, 24h, 49h, 71h, 145h, 167h - see Fig. 6) for XRD and SEM  
536 analysis. At each timepoint, 0.5 – 1 L seawater was collected from the tank sampling port or from the center of the  
537 aquaria. In cases where precipitation had visibly settled at the bottom of the aquaria, this material was stirred into the  
538 water column before sampling. We note that material that settled to the bottom of the large tanks was not directly  
539 collected, and that only a subset of precipitation was collected at each time point, such that later timepoints may  
540 include solids that had precipitated at the beginning of the experiment. The filtered seawater was immediately  
541 analyzed for TA and pH via Ross electrode because the heightened pH was out of the range of spectrophotometric  
542 methods. Bottle samples of filtered seawater were not able to be analyzed at NOAA PMEL due to the continued  
543 precipitation of CaCO<sub>3</sub> after filtration and preservation. Both XRD and SEM results showed the dominance of  
544 Mg(OH)<sub>2</sub> precipitation immediately after the alkalinity addition and the corresponding increase in pH and  $\Omega_{\text{aragonite}}$   
545 (to a value of around 30). The Mg(OH)<sub>2</sub> precipitation at this stage was thick, slurry-like, and difficult to  
546 appropriately rinse. Broad peaks associated with brucite in the 0 and 3 hr time points may reflect that these signals  
547 were partially obscured by the presence of other salts, and a sharp peak in the 0 hr time point  $\sim 27^\circ 2\theta$  is likely



548 associated with NaCl. Within hours of the NaOH addition, the runaway  $\text{CaCO}_3$  precipitation began, characterized by  
 549 fine, light particulates in the water column and a sharp increase in turbidity. Within  $\sim 24$  hours of the NaOH addition,  
 550 most  $\text{Mg}(\text{OH})_2$  signals had disappeared, leaving only aragonite and calcite peaks in the XRD. The results of the  
 551 XRD analysis for the tank experiment are summarized in Figure 7, and the aquarium experiment showed similar  
 552 results (see Supplementary Materials). TA decreased throughout the precipitation of  $\text{Mg}(\text{OH})_2$  and  $\text{CaCO}_3$ , and was  
 553 below that of the initial seawater within 24 hours of the NaOH addition. In the tank experiment, the initial TA (2025  
 554  $\mu\text{mol}/\text{kg}$ ) was raised by 3305  $\mu\text{mol}/\text{kg}$ . Within 3 days the TA had decreased to 1583  $\mu\text{mol}/\text{kg}$  and continued to  
 555 decrease through the termination of the experiment to 1253  $\mu\text{mol}/\text{kg}$  10 days after the addition of NaOH. The DIC,  
 556 which was initially measured at 1938  $\mu\text{mol}/\text{kg}$ , decreased to 720  $\mu\text{mol}/\text{kg}$  by the end of the experiment. This  
 557 experiment shows that runaway  $\text{CaCO}_3$  can result in a significant loss of both efficiency of alkalinity dosing for  
 558 OAE projects and of storage of carbon in the form of DIC. A figure of time-series data collected during the tank  
 559 experiment is available in the Supplementary Materials.



560  
 561 **Figure 6:** (a) XRD analysis of particulates filtered from seawater after the addition of enough NaOH to raise the  
 562 bulk seawater  $\text{pH}_T$  to 10.3 showed mineral precipitation initially dominated by  $\text{Mg}(\text{OH})_2$  before it was overtaken by  
 563  $\text{CaCO}_{3,\text{arag}}$ . The shaded grey vertical bars highlight several peaks characteristic of brucite which typically disappear  
 564 after 24 hours, and the shaded blue bars represent several aragonite peaks which appear between 3 and 24 hours.  
 565 Representative SEM images show (b)  $\text{CaCO}_{3,\text{arag}}$  at the end of the experiment, and (c)  $\text{Mg}(\text{OH})_2$  captured  $\sim 3$  hours  
 566 after the NaOH addition. Photographs of the tank experiment show seawater (d)  $\sim 3$  hours after the NaOH addition,  
 567 when runaway  $\text{CaCO}_3$  precipitation became visually apparent, (e) during NaOH addition into still water (i.e.,  
 568 without the use of stirrers, circulation pumps, or air bubblers to break up and redissolve  $\text{Mg}(\text{OH})_2$ ), and (f) before  
 569 NaOH addition.

570 In summary, the presence and duration of brucite precipitation upon addition of 0.5 M aqueous NaOH depends on  
 571 the ratio of the NaOH addition rate to the local dilution rate in the receiving waters. Future research using flow  
 572 through tanks could help identify thresholds below which brucite precipitation can be avoided or limited, and the  
 573 immediate formation of  $\text{Mg}(\text{OH})_2$  may be reversible, as also noted by Suitner et al. (2023) and Cyronak et al.  
 574 (2023). At the given initial seawater conditions, the threshold for aragonite precipitation began at an  $\Omega_{\text{arag}}$  of 30,  
 575 corresponding to  $\text{pH}_T > 10.0$ , and continued as  $\Omega_{\text{arag}}$  decreased to  $\sim 5.2$ . This threshold corresponded to an increase in  
 576 TA of  $> 2270 \mu\text{mol}/\text{kg}$ . The potential for runaway aragonite precipitation may be reduced by active mixing at the  
 577 point of NaOH introduction, maintaining a mixing volume below bulk seawater  $\text{pH}_T$  of 10.0, and allowing for  
 578 appropriate dilution in flow-through conditions, particularly on timescales of hours after alkalinity addition.

579 Additional characterization of runaway precipitation thresholds at varying temperatures, salinities, and suspended  
580 particulate conditions will allow for OAE implementation designs that best avoid this potential risk to OAE  
581 efficiency and ecosystem perturbation. We note that these results are only valid for experiments that are open to the  
582 atmosphere allowing for exchange of CO<sub>2</sub> across the air-sea boundary using an aqueous hydroxide feedstock for  
583 alkalinity, and are not comparable to experiments such as closed bottle incubations, where sustained conditions of  
584 high  $\Omega_{\text{arag}}$  may result in precipitation at different thresholds. We also note that we do not assume zero aragonite  
585 precipitation at conditions below the stated thresholds, but that potential precipitation is not readily detectable with  
586 our experimental setup. For example, heterogeneous CaCO<sub>3</sub> precipitation events, such as may occur on suspended  
587 sediments in the water column, have been suggested through characteristic changes in seawater TA/DIC ratios in  
588 cases of riverine inputs and bottom sediment resuspension (Bustos-Serrano et al., 2009; Wurgaft et al., 2016; 2021).  
589 Suspended sediments in the context of OAE project sites could influence OAE efficiency and the potential for  
590 runaway precipitation and should be included in future studies (Bach, 2023). The thresholds determined in this study  
591 are significantly higher than those of some mineral-based OAE studies, including precipitation after an increase in  
592 TA of ~500  $\mu\text{mol/kg}$  using CaO and Ca(OH)<sub>2</sub> mineral additions (Moras et al., 2022). Hartmann et al. (2022) noted  
593 precipitation resulting from alkalinity additions of >600  $\mu\text{mol/kg}$  Mg(OH)<sub>2</sub>, and found that alkaline solutions  
594 avoided carbonate precipitation better than reactive alkaline particle additions to seawater. Suitner et al. (2023)  
595 suggested that alkalinity additions > 2000  $\mu\text{mol/kg}$  could be achievable given sufficient dilution to avoid runaway  
596 precipitation. Together, these studies highlight the need to expand research into runaway precipitation to  
597 characterize potential inefficiencies in OAE, particularly in in-situ experiments to establish relationships applicable  
598 to ocean environments.

## 599 **5 Summary and Future Work**

600 These results demonstrate that ocean alkalinity enhancement using aqueous sodium hydroxide in seawater results in  
601 CO<sub>2</sub> removal from air at an efficiency of 0.75 ( $\pm 0.04$ ) – 0.92 ( $\pm 0.10$ ), with 90% equilibration typically achieved  
602 within 7 - 9 weeks (still surface water with ~16 L/min subsurface circulation through UV arrays) to 3 - 5 weeks  
603 (with the addition of ambient air bubbling into the bottom of each tank) of the initial addition when performed in  
604 ~6000 L tanks with seawater-air contact areas of around 4.6 m<sup>2</sup>. These results are in general agreement with ratios  
605 noted in Burt et al. (2021), He and Tyka (2023), and Wang et al., (2023). Here, uncertainties are driven by sensor  
606 precision and temporal resolution in discrete DIC and TA sampling, the limited number of experiments with  
607 minimal opportunities for duplicates or replicates, and poorly constrained data on mixing, circulation, and air  
608 bubbling rates. Ongoing experiments seek to improve each of these conditions and should particularly focus on  
609 constraining the movement of water within a given tank to improve air-sea equilibration estimates and to allow for  
610 better extrapolation from tank to field experiments. In addition, a focus of ongoing and future work is to provide rate  
611 estimates for the uptake of atmospheric CO<sub>2</sub> in response to an NaOH addition, allowing for fitting and extrapolation  
612 of a shortened experiment to equilibration with the atmosphere.

613 We relied on several methods to constrain seawater carbonate chemistry. The tank-scale experiments primarily  
614 relied on discrete (at most daily) DIC and TA sampling (NOAA PMEL), paired with daily measurements from  
615 spectrophotometric pH systems (SAMI-pH and a semi-automated benchtop spec-pH system following Carter et al.  
616 (2013)) and local TA measurements. With appropriate calibration or correction of the spec-pH systems relative to  
617 CRM, there was no significant difference in carbonate calculations using the NOAA PMEL DIC-TA or spec-pH-  
618 local TA pairings, though the latter case typically produced larger uncertainties. Aquaria experiments relied on a  
619 standard glass pH electrode (at most daily, corrected to spectrophotometric systems) with discrete (at most daily) TA  
620 measurements, which provided reasonable data relative to the tank experiments. As a result, ongoing tank-scale  
621 experiments have limited the volume of discrete DIC and TA samples collected for analysis at NOAA PMEL to  
622 allow for faster and less expensive monitoring via spec-pH and local TA titrations. However, we note that the major  
623 limitation in this measurement pathway lies in the spec-pH method, which is typically limited to pH<sub>T</sub> measurements  
624 ranging from 7 – 9 for the meta-cresol purple indicator dye used. While our measurements retained some sensitivity

625 up to  $\text{pH}_T$  9.5, such a method should typically be considered unreliable at these  $\text{pH}_T$  values, and we relied on  
626 frequent correction to CRM and comparison with DIC/TA samples. Thymol blue is an alternative  
627 spectrophotometric  $\text{pH}_T$  indicator dye with sensitivity over the higher  $\text{pH}_T$  conditions observed during these initial  
628 trials and will be assessed for future experiments (Zhang and Byrne, 1996; Liu et al., 2006).

629 Aqueous NaOH with concentrations as high as 0.5 M can be added directly to turbulent seawater with only limited  
630 observable precipitation of  $\text{Mg}(\text{OH})_2$ . In these conditions this precipitated mineral rapidly redissolves on the  
631 timescales of minutes to seconds. Improved control over the NaOH dosing rate (in our tank experiments, ~50 mL  
632 NaOH/min) and the turbulence of the receiving water through metered flow through experiments will be valuable in  
633 extrapolating to field conditions. This precipitation is detectable both visually and through turbidity measurements  
634 and implies that straightforward measurement of pH and turbidity at the dispersal site can be used to adjust the  
635 alkalinity dispersal rate according to local mixing conditions such that  $\text{Mg}(\text{OH})_2$  precipitation is avoided and/or  
636 redissolves when it occurs. No significant  $\text{CaCO}_3$  precipitation was observed at  $\text{pH} < 10.0$  or  $\Omega_{\text{aragonite}} < 30.0$ .  
637 Runaway  $\text{CaCO}_3$  precipitation was observed above these thresholds, where a massive precipitation and settling of  
638  $\text{Mg}(\text{OH})_2$  and  $\text{CaCO}_3$  solids results in less alkalinity in the overlying water than at the starting condition. pH and  
639 turbidity sensing combined with discrete TA measurements could be used as a feedback signal for alkalinity dosing  
640 into seawater to ensure that the local maximum thresholds at the dispersal location do not approach or exceed  
641 conditions that promote significant  $\text{CaCO}_3$  precipitation. We note that future investigations seeking to better  
642 approximate field conditions should take into account seasonal and tidal shifts in temperature and salinity, and  
643 varying conditions of suspended sediment in the water column, including that of aerial dust, terrestrial runoff, and  
644 resuspended bottom sediments.

645 In these experiments, the seawater was filtered and bleach treated prior to experiments to limit biological growth,  
646 and both tank and aquaria experiments were conducted indoors with limited light. Nevertheless, in most  
647 experiments, biological growth was observed after a few weeks, including cyanobacteria and coccolithophores. A  
648 series of experiments are underway to test the difference in  $\text{CO}_2$  removal efficiency for two side-by-side tanks, both  
649 of which are dosed with NaOH, but only one of which was bleached. Preliminary results show minimal difference  
650 between the bleached and unbleached tanks, indicating these experiments are applicable to real-world conditions, at  
651 least for regions with biological communities similar to that of Long Island Sound, but further investigation is  
652 warranted.

653 A focus of future work is to consider the potential impact of the SEAMATE process on local ocean acidification  
654 mitigation efforts. We note that in each constrained tank and aquarium experiment, the  $\text{pH}_T$  at equilibrium exceeds  
655 the initial  $\text{pH}_T$  value prior to the addition of alkalinity. A controlled release of alkalinity could theoretically be  
656 configured to maintain a locally elevated  $\text{pH}_T$  value relative to pre-alkaline conditions, with potential uses in  
657 aquaculture and hatchery environments.

658 These results provide clear and practical guidelines for MRV for OAE implementations employing aqueous  
659 alkalinity. First, carbonate chemistry and turbidity measurements at the alkalinity dispersal location can ensure that  
660 seawater parameters such as pH and  $\Omega_{\text{aragonite}}$  remain within pre-determined safe bounds and that unwanted  
661 precipitation is avoided. Second, for a given OAE deployment, where ocean models provide a reasonable certainty  
662 about the fraction of the alkalinity plume remaining in the surface over weeks to months, the  $\text{CO}_2$  removal efficiency  
663 and timescale for air-seawater equilibration provided by our experiments can place a lower bound on the amount of  
664  $\text{CO}_2$  removal expected from that OAE intervention. Expanding these studies from tank scale to mesocosm and field  
665 experiments will be crucial to understanding biological impacts and constraining realistic air-sea interactions in  
666 response to this type of OAE (Oschlies et al., 2023).

667 **Data availability**

668 Data are described in the manuscript and provided Supplementary Materials, which includes a .csv file with  
669 processed sensor and sample time-series data at hourly resolution.

#### 670 **Author contribution**

671 MDE and BRC designed the experiments and MCR carried them out with support from NH, CS, and XL. JH  
672 provided support on experimental setup and instrumentation. MCR prepared the manuscript with contributions from  
673 all co-authors.

#### 674 **Competing interests**

675 MCR is Lead Oceanographer and Head of MRV at Ebb Carbon, Inc. MDE is Co-Founder and Chief Scientific  
676 Advisor at Ebb Carbon, Inc.

#### 677 **Acknowledgements**

678 We would like to thank Stephen Abrams and Thomas Wilson at Stony Brook University Flax Pond Marine Lab for  
679 technical assistance in experiment setup. We thank Chris Ikeda and Susan Curless of NOAA PMEL for support in  
680 discrete sample analysis. We thank Mike Tyka for productive discussions. We thank Eyal Wurgaft for assistance in  
681 TA titrations.

#### 682 **Funding**

683 We acknowledge funding from The Grantham Foundation for the Protection of the Environment under the SEA  
684 MATE (Safe Elevation of Alkalinity for the Mitigation of Acidification Through Electrochemistry) grant. In  
685 addition, this research used the XRD facility of the Center for Functional Nanomaterials (CFN), which is a U.S.  
686 Department of Energy Office of Science User Facility, at Brookhaven National Laboratory under Contract No. DE-  
687 SC0012704. BRC and JH were funded through the Cooperative Institute for Climate, Ocean, and Ecosystem  
688 Studies (CICOES) under NOAA Cooperative Agreement NA20OAR4320271 and supported by NOAA's PMEL.

#### 689 **References**

- 690  
691 Albright, R., Caldeira, L., Hoffelt, J., Kwiatkowski, L., Maclaren, J.K., Mason, B.M., Nebuchina, Y. et al.: Reversal  
692 of ocean acidification enhances net coral reef calcification. *Nature*, 531, no. 7594: 362-365, 2016.  
693 Bach, L.T.: The additionality problem of ocean alkalinity enhancement. *Biogeosciences*, 21, 261-277, 2024.  
694 Bach, L. T., Gill, S.J., Rickaby, R.E.M., Gore, S., and Renforth, P.: CO<sub>2</sub> removal with enhanced weathering and  
695 ocean alkalinity enhancement: potential risks and co-benefits for marine pelagic ecosystems. *Frontiers in*  
696 *Climate*, 1, 7, 2019.  
697 Bainbridge, Z., Lewis, S., Bartley, R., Fabricius, K., Collier, C., Waterhouse, J., Garzon-Garcia, A., Robson, B.,  
698 Burton, J., Wenger, A., and Brodie, J: Fine sediment and particulate organic matter: A review and case study on  
699 ridge-to-reef transport, transformations, fates, and impacts on marine ecosystems. *Marine Pollution Bulletin*  
700 135, pp. 1205-1220. 2018  
701 Berner, R. A., Lasaga, A.C., and Garrels, R.M.: Carbonate-silicate geochemical cycle and its effect on atmospheric  
702 carbon dioxide over the past 100 million years. *Am. J. Sci.:(United States)* 283, no. 7, 1983.  
703 Boettcher, M., Chai, F. Cullen, J., Goeschl, T., Lampitt, R., Lenton, A., Oeschies, A. et al.: High level review of a  
704 wide range of proposed marine geoengineering techniques. *GESAMP Working Group Reports and Studies*, 41,  
705 2019.  
706 Brodersen, K.E., Hammer, K.J., Schrammeyer, V., Floytrup, A., Rasheed, M.A., Ralph, P.J., Köhl, M., and Pederson,  
707 O.: Sediment resuspension and deposition on seagrass leaves impedes internal plant aeration and promotes  
708 phytotoxic H<sub>2</sub>S intrusion. *Frontiers in Plant Science* 8. 2017  
709 Burt, D.J., Fröb, F., & Ilyina, T.: The sensitivity of the marine carbonate system to regional ocean alkalinity  
710 enhancement. *Frontiers in Climate* 3, 624075. 2021

711 Bustos-Serrano, H., Morse, J.W., & Millero, F.J.: The formation of whittings on the Little Bahama Bank. *Marine*  
712 *Chemistry* 113, no. 1-2, pp. 1-8. 2009

713 Butenschön, M., Lovato, T., Masina, S., Caserini, S., and Grosso, M.: Alkalinization scenarios in the Mediterranean  
714 Sea for efficient removal of atmospheric CO<sub>2</sub> and the mitigation of ocean acidification. *Frontiers in Climate* 3,  
715 614537. 2021

716 Carter, B. R., J. A. Radich, H. L. Doyle, and A. G. Dickson.: An automated system for spectrophotometric seawater  
717 pH measurements. *Limnology and Oceanography: Methods*, 11, no. 1: 16-27, 2013.

718 Caserini, S., Storni, N., & Grosso, M.: The availability of limestone and other raw materials for ocean alkalinity  
719 enhancement. *Global Biogeochemical Cycles*, 36, e2021GB007246. <https://doi.org/10.1029/2021GB007246>,  
720 2022.

721 Cross, J.N., Sweeney, C., Jewett, E.B., Feely, R.A., McElhany, P., Carter, B., Stein, T., Kitch, G.D., and Gledhill,  
722 D.: Strategy for NOAA carbon dioxide removal research: A white paper documenting a potential NOAA CDR  
723 science strategy as an element of NOAA's Climate Interventions Portfolio. NOAA Special Report. NOAA,  
724 Washington, DC. DOI: 10.25923/gzke-8730. 2023

725 Cyronak, T., Albright, R., and Bach, L.: Field experiments in  
726 ocean alkalinity enhancement research. *State of the Planet*, 2-oae2023 (7). 2023.

727 de Lannoy, C.-F., Eisaman, M.D., Jose, A., Karnitz, S.D., DeVaul, R.W., Hannun, K., and Rivest, J.L.B.: Indirect  
728 ocean capture of atmospheric CO<sub>2</sub>: Part I. Prototype of a negative emissions technology. *International journal of*  
729 *greenhouse gas control*, 70: 243-253, 2018.

730 Dickson, A. G.: An exact definition of total alkalinity and a procedure for the estimation of alkalinity and total  
731 inorganic carbon from titration data. *Deep Sea Research Part A. Oceanographic Research Papers*, 28(6), 609–  
732 623, 1981.

733 Dickson, A. G.: The development of the alkalinity concept in marine chemistry. *Marine Chemistry*, 40(1–2), 49–63,  
734 1992.

735 Dickson, A.G.: Thermodynamics of the dissociation of boric acid in synthetic seawater from 273.15 to 318.15 K.  
736 *Deep Sea Research Part A. Oceanographic Research Papers*, 37, no. 5: 755-766, 1990.

737 Dickson, A.G., Sabine, C.L., and Christian, J.R.: Guide to best practices for ocean CO<sub>2</sub> measurements. North Pacific  
738 Marine Science Organization, 2007.

739 Eisaman, M. D., Parajuly, K., Tuganov, A., Eldershaw, C., Chang, N.,  
740 Littau, K. A. CO<sub>2</sub> Extraction from Seawater Using Bipolar Membrane Electrodialysis, *Energy Environ. Sci.*, 5:  
741 7346. <https://doi.org/10.1039/c2ee03393c>. 2012.

742 Eisaman, M. D.; Rivest, J. L. B.; Karnitz, S. D.; De Lannoy, C.-F.; Jose, A.; DeVaul, R. W.; Hannun, K. Indirect  
743 Ocean Capture of Atmospheric CO<sub>2</sub>: Part II. Understanding the Cost of Negative Emissions. *International*  
744 *Journal of Greenhouse Gas Control*, 70: 254–261, <https://doi.org/10.1016/j.ijggc.2018.02.020>, 2018.

745 Eisaman, M. D., Geilert, S., Renforth, P., Bastianini, L., Campbell, J., Dale, A. W., Foteinis, S., Grasse, P., Hawrot,  
746 O., Löscher, C. R., Rau, G. H., and Rønning, J.: Assessing the technical aspects of ocean-alkalinity-  
747 enhancement approaches, in: *Guide to Best Practices in Ocean Alkalinity Enhancement Research*, edited by:  
748 Oschlies, A., Stevenson, A., Bach, L. T., Fennel, K., Rickaby, R. E. M., Satterfield, T., Webb, R., and Gattuso,  
749 J.-P., Copernicus Publications, *State Planet*, 2-oae2023, 3, <https://doi.org/10.5194/sp-2-oae2023-3-2023>, 2023.

750 Feely, R.A., Alin, S., Carter, B., Bednaršek, N., Hales, B., Chan, F., Hill, T.M., Gaylord, B., Sanford, E., Byrne,  
751 R.H., Sabine, C.L., Greeley, D., Juranek, L., Chemical and biological impacts of ocean acidification along the  
752 west coast of North America, *Estuarine, Coastal and Shelf Science*, doi: 10.1016/j.ecss.2016.08.043, 2016.

753 Feng, E. Y., Koeve, W., Keller, D.P., and Oschlies, A.: Model-Based Assessment of the CO<sub>2</sub> Sequestration Potential  
754 of Coastal Ocean Alkalinization. *Earth's Future*, 5, no. 12: 1252-1266, 2017.

755 Fennel, K., Long, M.C., Algar, C., Carter, B., Keller, D., Laurent, A., Mattern, J.P., Musgrave, R., Oschlies, A.,  
756 Ostiguy, J., Palter, J.B., and Whitt, D.B.: Modeling considerations for research on Ocean Alkalinity  
757 Enhancement (OAE). *State of the Planet*, 2-oae2023 (9). 2023. Ferderer, A., Chase, Z., Kennedy, F., Schulz,  
758 K.G., and Bach, L.T.: Assessing the influence of ocean alkalinity enhancement on a coastal phytoplankton  
759 community. *Biogeosciences* 19, no. 23: 5375-5399, 2022.

760 Friis, K.; Körtzinger, A.; Wallace, D. W. R. The Salinity Normalization of Marine Inorganic Carbon Chemistry  
761 Data. *Geophys. Res. Lett.*, 30 (2). <https://doi.org/10.1029/2002GL015898>, 2003.

762 Groen, A., Kittu, L., Ortiz Cortes, J., Schulz, K., and Riebesell, U.: Assessing the response of particulate organic  
763 matter stoichiometry to ocean alkalisation. *Ocean Visions Summit*, Atlanta, Georgia, USA,  
764 2023ocvi.conf27171G. 4-6 April 2023

765 Hartmann, J., Suitner, N., Lim, C., Schneider, J., Marín-Samper, L., Arístegui, J., Renforth, P., Taucher, J., and  
766 Riebesell, U.: Stability of alkalinity in ocean alkalinity enhancement (OAE) approaches—consequences for  
durability of CO<sub>2</sub> storage. *Biogeosciences* 20, no. 4: 781-802, 2023.

767 Harvey, L.: Mitigating the atmospheric CO<sub>2</sub> increase and ocean acidification by adding limestone powder to  
768 upwelling regions, *Journal of Geophysical Research: Oceans*, 113, 2008.

769 He, J. and Tyka, M. D.: Limits and CO<sub>2</sub> equilibration of near-coast alkalinity enhancement, *Biogeosciences*, 20, 27–  
770 43, <https://doi.org/10.5194/bg-20-27-2023>, 2023.

771 Ho, D. T., Bopp, L., Palter, J.B., Long, M.C., Boyd, P.W., Neukermans, G., and Bach, L.T.: Monitoring, reporting,  
772 and verification for ocean alkalinity enhancement. *State of the Planet*, 2-oae2023 (12). 2023. Ilyina, T., Wolf-  
773 Gladrow, D., Munhoven, G., and Heinze, C.: Assessing the potential of calcium-based artificial ocean  
774 alkalization to mitigate rising atmospheric CO<sub>2</sub> and ocean acidification, *Geophysical Research Letters*, 40,  
775 5909-5914, 2013.

776 IPCC: Summary for Policymakers. In: *Climate Change 2021: The Physical Science Basis*, Contribution of Working  
777 Group I to the Sixth Assessment Report of the Intergovernmental Panel on Climate Change, edited by: Masson-  
778 Delmotte, V., Zhai, P., Pirani, A., Connors, S. L., Péan, C., Berger, S., Caud, N., Chen, Y., Goldfarb, L., Gomis,  
779 M. I., Huang, M., Leitzell, K., Lonnoy, E., Matthews, J. B. R., Maycock, T. K., Waterfield, T., Yelekçi, O., Yu,  
780 R., and Zhou, B.: Cambridge University Press, Cambridge, United Kingdom and New York, NY, USA, 3–32,  
781 <https://doi.org/10.1017/9781009157896.001>, 2022.

782 Isson, T. T., Planavsky, N. J., Coogan, L. A., Stewart, E. M., Ague, J. J., Bolton, E. W., et al.: Evolution of the  
783 global carbon cycle and climate regulation on earth. *Global Biogeochemical Cycles*, 34, e2018GB006061.  
784 <https://doi.org/10.1029/2018GB006061>, 2020.

785 Johnson, K.M., King, A.E., and Sieburth, J.M.: Coulometric TCO<sub>2</sub> analyses for marine studies: An introduction.  
786 *Marine Chemistry* 16, pp. 61-82. 1985.

787 Jones, D.C., Ito, T., Takano, Y., and C.-W Hsu, C.-W.: Spatial and seasonal variability of the air-sea equilibration  
788 timescale of carbon dioxide. *Global Biogeochemical Cycles*, 28(11), 1163–1178,  
789 <https://doi.org/10.1002/2014GB004813>, 2014.

790 Khesghi, H. S.: Sequestering atmospheric carbon dioxide by increasing ocean alkalinity, *Energy*, 20, 915-922, 1995.

791 Köhler, P., Hartmann, J., and Wolf-Gladrow, D.A.: Geoengineering potential of artificially enhanced silicate  
792 weathering of olivine. *Proceedings of the National Academy of Sciences* 107, no. 47: 20228-20233, 2010.

793 La Plante, E., Chen, X., Bustillos, S., Bouissonnie, A., Traynor, T., Jassby, D., Corsini, L., Simonetti, D., and Sant,  
794 G.: Electrolytic seawater mineralization and the mass balances that demonstrate carbon dioxide removal. *ACS*  
795 *EST Engg.* <https://doi.org/10.1021/acsestengg.3c00004>, 2023.

796 Lee, K., Kim, T.-W., Byrne, R.H., Millero, F.J., Feely, R.A., and Liu, Y.-M.: The universal ratio of boron to  
797 chlorinity for the North Pacific and North Atlantic oceans. *Geochimica et Cosmochimica Acta* 74, no. 6: 1801-  
798 1811, 2010.

799 Lewis, E., Wallace, D., & Allison, L. J.: Program developed for CO<sub>2</sub> system calculations.  
800 <https://doi.org/10.2172/639712>, 1998.

801 Liu, X., Wang, Z.A., Byrne, R.H., Kaltenbacher, E.A., and Bernstein, R.E.: Spectrophotometric measurements of  
802 pH in-situ: laboratory and field evaluations of instrumental performance. *Environmental Science & Technology*  
803 40, no. 16, 5026-5044. 2006

804 Lu, X., Ringham, M., Hirtle, N., Hillis, K., Shaw, C., Herndon, J., Carter, B.R., and Eisaman, M.D.:  
805 Characterization of an Electrochemical Approach to Ocean Alkalinity Enhancement. In *AGU Fall Meeting*  
806 *Abstracts*, vol. 2022, pp. GC31C-01. 2022.

807 Lueker, T.J., Dickson, A.G., and Keeling, C.D.: Ocean pCO<sub>2</sub> calculated from dissolved inorganic carbon, alkalinity,  
808 and equations for K<sub>1</sub> and K<sub>2</sub>: validation based on laboratory measurements of CO<sub>2</sub> in gas and seawater at  
809 equilibrium. *Marine chemistry* 70, no. 1-3: 105-119, 2000.

810 Minx, J.C., Lamb, W.F., Callaghan, M.W., Fuss, S., Hilaire, J., Creutzig, F., Amann, T., et al.: Negative  
811 emissions—Part 1: Research landscape and synthesis. *Environmental Research Letters* 13, no. 6: 063001, 2018.

812 Montserrat, F., Renforth, P., Hartmann, J., Leermakers, M., Knops, P., and Meysman, F.J.R.: Olivine dissolution in  
813 seawater: implications for CO<sub>2</sub> sequestration through enhanced weathering in coastal environments.  
814 *Environmental Science & Technology* 51, no. 7: 3960-3972, 2017.

815 Moras, C.A., Bach, L.T., Cyronak, T., Joannes-Boyau, R., and Schulz, K.G.: Ocean alkalinity enhancement—  
816 avoiding runaway CaCO<sub>3</sub> precipitation during quick and hydrated lime dissolution. *Biogeosciences* 19, no. 15:  
817 3537-3557, 2022.

818 National Academies of Sciences, Engineering, and Medicine. A research strategy for ocean-based carbon dioxide  
819 removal and sequestration. 2021.

820 National Academies of Sciences, Engineering, and Medicine. Negative Emissions Technologies and Reliable  
821 Sequestration: A Research Agenda. 2018.

822 Nduagu, E. "Production of  $Mg(OH)_2$  from Mg-silicate rock for  $CO_2$  mineral sequestration. Dissertation for Abo  
823 Akademi University, 2012. Oschlies, A., Bach, L., Rickaby, R., Satterfield, T., Webb, R. M., and Gattuso, J.-P.:  
824 Climate targets, carbon dioxide removal and the potential role of Ocean Alkalinity Enhancement. *State of the*  
825 *Planet*, 2-oae2023 (1). 2023.

826 Pierrot, D., Lewis, E., and Wallace, D.W.R.: MS Excel program developed for  $CO_2$  system calculations.  
827 ORNL/CDIAC-105a. Carbon Dioxide Information Analysis Center, Oak Ridge National Laboratory, U.S.  
828 Department of Energy, Oak Ridge, Tennessee, 2006.

829 Rau, G.H.: Electrochemical splitting of calcium carbonate to increase solution alkalinity: Implications for mitigation  
830 of carbon dioxide and ocean acidity. *Environmental science & technology* 42, no. 23: 8935-8940, 2008.

831 Renforth, P., and Henderson, G.: Assessing ocean alkalinity for carbon sequestration. *Reviews of Geophysics* 55,  
832 no. 3: 636-674, 2017.

833 Rigopoulos, I., Harrison, A.L., Delimitis, A., Ioannou, I., Efstathiou, A.M., Kyratsi, T., and Oelkers, E.H. : Carbon  
834 sequestration via enhanced weathering of peridotites and basalts in seawater. *Applied Geochemistry* 91: 197-  
835 207, 2018.

836 Rueda, O., Mogollón, J.M., Tukker, A., and Scherer, L.: Negative-emissions technology portfolios to meet the 1.5°  
837 C target. *Global Environmental Change* 67: 102238, 2021.

838 Rogelj, J., Popp, A., Calvin, K. V., Luderer, G., Emmerling, J., Gernaat, D., Fujimori, S., Strefler, J., Hasegawa, T.,  
839 Marangoni, G., Krey, V., Kriegler, E., Riahi, K., van Vuuren, D. P., Doelman, J., Drouet, L., Edmonds, J.,  
840 Fricko, O., Harmsen, M., Havlík, P., Humpenöder, F., Stehfest, E., and Tavoni, M.: Scenarios towards limiting  
841 global mean temperature increase below 1.5 °C, *Nat. Clim. Change*, 8, 325–332, [https://doi.org/10.1038/s41558-](https://doi.org/10.1038/s41558-018-0091-3)  
842 018-0091-3, 2018.

843 Schulz, K. G., Bach, L. T., and Dickson, A. G.: Seawater carbonate system considerations for ocean alkalinity  
844 enhancement research: theory, measurements, and calculations. *State of the Planet*, 2-oae2023 (2). 2023..

845 Shaw, C., Ringham, M.C., Lu, X., Carter, B.R., Eisaman, M.D., and Tyka, M.: Understanding the Kinetics of  
846 Electrochemically derived Magnesium Hydroxide for Ocean Alkalinity Enhancement. In AGU Fall Meeting  
847 Abstracts, vol. 2022, pp. GC32I-0713. 2022.

848 Song, S., Wang, Z.A., Gonnee, M.E., Kroeger, K.D., Chu, S.N., Li, D., and Liang, H.: An important  
849 biogeochemical link between organic and inorganic carbon cycling: Effects of organic alkalinity on carbonate  
850 chemistry in coastal waters influenced by intertidal salt marshes. *Geochimica et Cosmochimica Acta* 275:123-  
851 139, 2020.

852 Suintner, N., Faucher, G., Lim, C., Schneider, J., Moras, C.A., Riebesell, U., and Hartmann, J.: Ocean alkalinity  
853 enhancement approaches and the predictability of runaway precipitation processes- Results of an experimental  
854 study to determine critical alkalinity ranges for safe and sustainable application scenarios. *EGU*sphere  
855 [preprint], <https://doi.org/10.5194/egusphere-20223-2611>, 2023

856 Tyka, M.D., Arsdale, C.V., and Platt, J.C.:  $CO_2$  capture by pumping surface acidity to the deep ocean. *Energy &*  
857 *Environmental Science* 15, no. 2: 786-798, 2022.

858 Van Heuven, S., Pierrot, D., Rae, J., Lewis, E., & Wallace, D.: MATLAB program developed for  $CO_2$  system  
859 calculations. ORNL/CDIAC-105b, 530, 2011.

860 Vitillo, J. G., Eisaman, M.D., Aradóttir, E.S.P., Passarini, F., Wang, T., and Sheehan, S.W.: The role of carbon  
861 capture, utilization and storage for economic pathways that limit global warming to below 1.5° C." *Iscience*:  
862 104237, 2022.

863 Wang, H., Pilcher, D. J., Kearney, K. A., Cross, J. N., Shugart, O. M., Eisaman, M. D., & Carter, B. R.: Simulated  
864 impact of ocean alkalinity enhancement on atmospheric  $CO_2$  removal in the Bering Sea. *Earth's Future*, 11(1),  
865 e2022EF002816, 2023

866 Wang, Z. A. and Cai, W. J.: Carbon dioxide degassing and inorganic carbon export from a marsh-dominated estuary  
867 (the Duplin River): A marsh  $CO_2$  pump. *Limnol. Oceanogr.* 49, 341–354, 2004.

868 Wolf-Gladrow, D. A., Zeebe, R. E., Klaas, C., Körtzinger, A., & Dickson, A. G.: Total alkalinity: The explicit  
869 conservative expression and its application to biogeochemical processes. *Marine Chemistry*, 106(1–2), 287–  
870 300, 2007.

871

872 Wurgaft, E., Steiner, Z., Luz, B., and Lazar, B.: Evidence for inorganic precipitation of  $CaCO_3$  on suspended solids  
873 in the open water of the Red Sea, *Marine Chemistry*, 186, pp. 145–155, 2016.

874 Wurgaft, E., Wang, Z., Churchill, J., Dellapenna, T., Song, S., Du, J., Ringham, M., Rivlin, T., and Lazar, B.:  
875 Particle triggered reactions as an important mechanism of alkalinity and inorganic carbon removal in river  
876 plumes, *Geophysical Research Letters*, 48, e2021GL093178, <https://doi.org/10.1029/2021GL093178>, 2021

- 877 Zeebe, R.E., and Wolf-Gladrow, D.: CO<sub>2</sub> in seawater: equilibrium, kinetics, isotopes. Vol. 65, Gulf Professional  
878 Publishing. 2001.
- 879 Zhang, H., and Byrne, R.H.: Spectrophotometric pH measurements of surface seawater at in-situ conditions:  
880 absorbance and protonation behavior of thymol blue. *Marine Chemistry* 52, no. 1, pp. 17-25. 1996